



HAL
open science

Polyelectrolyte Brush Interacting with Ampholytic Nanoparticles as Coarse-Grained Models of Globular Proteins: Poisson–Boltzmann Theory

Tatiana O Salamatova, Mikhail Y Laktionov, Ekaterina B Zhulina, Oleg V. Borisov

► **To cite this version:**

Tatiana O Salamatova, Mikhail Y Laktionov, Ekaterina B Zhulina, Oleg V. Borisov. Polyelectrolyte Brush Interacting with Ampholytic Nanoparticles as Coarse-Grained Models of Globular Proteins: Poisson–Boltzmann Theory. *Biomacromolecules*, 2023, 24 (6), pp.2433-2446. 10.1021/acs.biomac.2c01153 . hal-04306914

HAL Id: hal-04306914

<https://univ-pau.hal.science/hal-04306914>

Submitted on 25 Nov 2023

HAL is a multi-disciplinary open access archive for the deposit and dissemination of scientific research documents, whether they are published or not. The documents may come from teaching and research institutions in France or abroad, or from public or private research centers.

L'archive ouverte pluridisciplinaire **HAL**, est destinée au dépôt et à la diffusion de documents scientifiques de niveau recherche, publiés ou non, émanant des établissements d'enseignement et de recherche français ou étrangers, des laboratoires publics ou privés.

1 Polyelectrolyte Brush Interacting with Ampholytic Nanoparticles as 2 Coarse-Grained Models of Globular Proteins: Poisson–Boltzmann 3 Theory

4 Tatiana O. Salamatova, Mikhail Y. Laktionov, Ekaterina B. Zhulina, and Oleg V. Borisov*



Cite This: <https://doi.org/10.1021/acs.biomac.2c01153>



Read Online

ACCESS |



Metrics & More

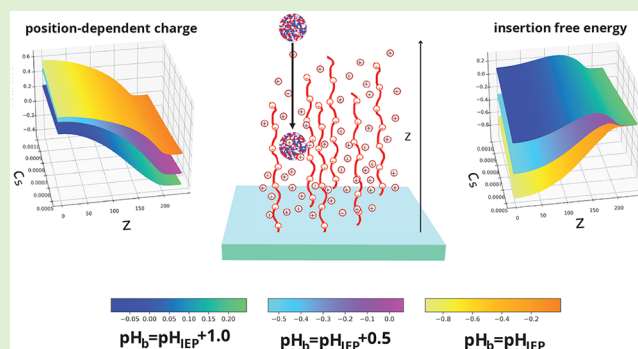


Article Recommendations



Supporting Information

5 **ABSTRACT:** The self-consistent field Poisson–Boltzmann frame-
6 work is applied to analyze equilibrium partitioning of ampholytic
7 nanoparticles (NPs) between buffer solution and polyelectrolyte
8 (PE) polyanionic brush. We demonstrate that depending on pH
9 and salt concentration in the buffer solution, interactions between
10 ionizable (acidic and basic) groups on the NP surface and
11 electrostatic field created by PE brush may either lead to the
12 spontaneous uptake of NPs or create an electrostatic potential
13 barrier, preventing the penetration of NPs inside PE brush. The
14 capability of PE brush to absorb or repel NPs is determined by the
15 shape of the insertion free energy that is calculated as a function of
16 NP distance from the grafting surface. It is demonstrated that, at a
17 pH value below or slightly above the isoelectric point (IEP), the
18 electrostatic free energy of the particle is negative inside the brush and absorption is thermodynamically favorable. In the latter case,
19 the insertion free energy exhibits a local maximum (potential barrier) at the entrance to the brush. An increase in pH leads to the
20 shallowing of the free energy minimum inside the brush and a concomitant increase in the free energy maximum, which may result in
21 kinetic hindering of NP uptake. Upon further increase in pH the insertion free energy becomes positive, making NP absorption
22 thermodynamically unfavorable. An increase in salt concentration diminishes the depth of the free energy minimum inside the brush
23 and eventually leads to its disappearance. Hence, in accordance with existing experimental data our theory predicts that an increase
24 in salt concentration suppresses absorption of NPs (protein globules) by PE brush in the vicinity of IEP. The interplay between
25 electrostatic driving force for NP absorption and osmotic repelling force (proportional to NP volume) indicates that for large NPs
26 with relatively small number of ionizable groups osmotic repulsion overcomes electrostatic attraction preventing thereby absorption
27 of NPs by PE brush.



1. INTRODUCTION

28 Electrostatic interactions between charged biomacromolecules
29 and proteins play an important role in many biological
30 processes.^{1–4} A better understanding of the interactions
31 between natural polyelectrolytes and proteins could thus
32 have both fundamental scientific importance and direct
33 medical implications. Synthetic polyelectrolytes (PEs) and
34 colloidal polyelectrolyte nanostructures could mimic natural
35 polyelectrolytes and their assemblies to unravel mechanisms of
36 molecular processes in living nature, including those of direct
37 medical relevance (e.g., inflammation or coagulation cascades).
38 On the other hand, colloidal PE nanostructures, such as
39 polyelectrolyte brushes, microgels, or block polyelectrolyte
40 micelles can be used in medical and biotechnological
41 applications (e.g., drug and gene delivery, inhibition of viral
42 infection, etc.).^{5–14}

43 PE brushes (layers of charged macromolecules terminally
44 attached to a planar substrate or to the surface of colloidal
45 particles and immersed in aqueous solution) play a prominent

46 role here, and their interactions with charged species have been
47 actively explored experimentally and theoretically (see ref 1 for
48 a comprehensive review). Planar, spherical, and cylindrical PE
49 brushes are distinguished according to the geometry of the
50 grafting surface. The latter closely mimic natural glycosami-
51 noglycans (GAGs) (e.g., aggrecan in articular cartilage,
52 envisioned as a cylindrical brush with keratan sulfate and
53 chondroitin sulfate side chains end-tethered to the core
54 protein¹⁵), or heparan-sulfate proteoglycans (HSPG) emanat-
55 ing from the cell surface.¹⁶

56 In living systems, globular proteins interact with charged
57 biomacromolecular assemblies that often have complex brush-

Received: September 22, 2022

Revised: March 21, 2023

58 like architectures (e.g., layers of bacterial extracellular
59 polysaccharides, endothelial glycocalyx, complexes of aggre-
60 canes with hyaluronic acid, etc.) comprising both weak
61 (carboxyl) and strong (sulfate) anionic groups. Synthetic PE
62 brushes can be formed by macromolecules comprising either
63 strong (permanently charged) or weak (pH-sensitive)
64 ionizable groups. Proteins, on the other hand, are weak
65 polyampholytes (PAs) that bear pH-sensitive cationic and
66 anionic groups on their surface. Hence, the net charge of the
67 protein globule depends on pH, and vanishes in the so-called
68 isoelectric point, pH_{IEP} , in which the net charges of cationic
69 and anionic groups exactly match each other. Hence, the
70 protein globule possesses a net positive or negative charge at
71 $pH \leq pH_{IEP}$ or $pH \geq pH_{IEP}$, respectively.

72 Under physiological conditions, biomacromolecular brushes
73 and most of globular proteins are similarly (negatively)
74 charged, so that their interactions could be mediated by the
75 Coulomb electrostatic repulsions. On the other hand, seminal
76 works of M. Ballauff and co-workers convincingly demon-
77 strated that synthetic polyanionic brushes can efficiently uptake
78 globular proteins above (on the “wrong side”) the IEP, that is,
79 when the PE brush and the protein are both negatively
80 charged.^{17–20} It was also demonstrated that absorption of the
81 proteins is efficient at low and suppressed at high ionic
82 strength due to the electrostatic nature of attraction between
83 similarly (negatively) charged PE brushes and proteins.

84 Two possible mechanisms were proposed to explain this
85 experimental observation: First, it was suggested that, due to
86 the Donnan equilibrium, pH inside the polyanionic brush may
87 be lower than pH_{IEP} even when pH in the buffer is higher than
88 pH_{IEP} so that the protein which is negatively charged in the
89 buffer, acquires positive charge inside the negatively charged
90 brush and, therefore, is spontaneously absorbed by the
91 brush.^{21–23} An alternative hypothesis exploits the fact that
92 cationic and anionic groups on the protein globule surface are
93 distributed inhomogeneously and give rise to “patches” of
94 positive and negative charges. Even when in total the globule is
95 charged negatively, adsorption of the brush-forming polyanions
96 on the (minority) patches of positive charge leads to the gain
97 in the electrostatic free energy which overcompensates the free
98 energy losses due to depletion from the negatively charged
99 patches.^{24,25} Recent experiments on complexation between
100 polyelectrolytes and green fluorescent protein mutants with
101 varied patchiness in the surface charge distribution²⁶
102 convincingly supports the importance of this mechanism of
103 polyelectrolyte–protein binding. Both hypotheses provide
104 qualitatively plausible explanation of the protein absorption
105 by similarly charged PE brushes though both lack quantitative
106 theoretical justification. Presumably, the reionization may
107 serve as the dominant driving force for binding of proteins
108 with fairly uniform (nonpatchy) distribution of cationic and
109 anionic groups on the globule surface, by strongly charged PE
110 brushes, including biological ones (e.g., HSPG). This is in a
111 line with results of numerical self-consistent field calculations
112 for protein-like ampholytic particles interacting with planar PE
113 brushes²³ and molecular dynamics simulations of short
114 ampholytic molecules interacting with a starlike PE.²⁷ At the
115 same time, the short-range nonelectrostatic interactions
116 between protein amino acid residues and the brush monomer
117 units could also be significant, and in a general case, absorption
118 of proteins by PE brushes is governed by both types of
119 interactions.²⁰

In our recent paper²⁸ we have demonstrated that charge
inversion due to reionization of a weak ampholytic nano-
particle (NP) upon insertion into a similarly charged PE brush
or microgel is a necessary but insufficient condition for the
negative balance in the differential free energy. In other words,
even if the NP, being negatively charged in the buffer, acquires
a positive charge inside the negatively charged brush, the net
ionic interaction balance may disfavor its uptake by the brush.
This qualitative conclusion was made on the basis of a simple
Donnan model that disregards the spatial distribution of an
electrostatic field inside the PE brush/microgel.

Advances in the theory of polyelectrolyte brushes^{29,30,32}
provide a full quantitative analytical description of the
electrostatic potential and local concentrations of mobile
ions inside and outside of planar PE brushes within the
accuracy of the Poisson–Boltzmann approximation. This
theoretical approach has been recently extended³³ to brushes
formed by branched polyelectrolytes that mimic natural
biomacromolecular brushes, and can be applied with
reasonable accuracy to PE brushes on surfaces of large
colloidal particles.³⁴

In this study, we focus exclusively on the electrostatic driving
forces with aim to unravel different mechanisms regulating
uptake of nanoparticles and globular proteins by PE brushes.
We assimilate globular proteins to weak polyampholytic
nanoparticles (NPs) with fixed volume and surface area
covered with both acidic and basic ionizable groups. Although
such coarse-graining of globular proteins is rather reduction-
istic, it could still illuminate general trends in the electrostatic
regulation of the protein–PE brush interactions. The aim of the
present paper is to implement the Poisson–Boltzmann
framework to analyze the position-dependent ionization and
insertion free energy of weak (pH-sensitive) polyampholytic
NPs, and to examine the effect of environmental conditions
(pH, salt concentration) and the brush grafting density on the
shape of insertion free energy curves. This approach provides
the distribution profiles of NPs inside the brush and may be
further used to access the diffusion rates of NPs through PE
brushes.

The rest of the paper is organized as follows: In section 2 we
introduce our theoretical model and present dominant
contributions to the NP free energy in the brush. A brief
summary on the Poisson–Boltzmann theory of PE brushes and
the review of electrostatic potential distribution is given in
section 3, while more detailed derivations are delegated to the
SI. Sections 3.1 and 3.2 are devoted to formulation of the
electrostatic and osmotic contributions to the insertion free
energy, respectively. The insertion free energy profiles
calculated under varied conditions for NPs with one anionic
and one cationic type of ionizable sites are presented in section
3.3. Finally, in section 4 we overview the results and outline
our conclusions.

2. METHOD

2.1. Model. We consider a polyampholytic nanoparticle
(NP), as a model of a protein in its globular conformation, that
comprises N_+ ionogenic groups (sites) capable of acquiring
positive (elementary) charge upon protonation, and N_-
monomer units capable of acquiring negative (elementary)
charge upon dissociation of hydrogen ion. The NP has volume
 V and ionizable groups are assumed to be evenly distributed on
its surface with area Σ .

180 In the general case, the NP might contain several types of
181 cationic and anionic ionogenic groups (i.e., amino acid
182 residues), each characterized by specific acidic ionization
183 constant $K_{i\pm}$. We ascribe the ionization constant K_{i-} to N_{i-}
184 anionic groups ($i_- = 1, 2, \dots$) and the ionization constant K_{i+} to
185 N_{i+} cationic groups ($i_+ = 1, 2, \dots$). Hence, the total number of
186 ionizable groups is

$$N_{\Sigma} = N_{+} + N_{-} = \sum_{i+} N_{i+} + \sum_{i-} N_{i-} \quad (1)$$

187
188 The NP is interacting with a polyelectrolyte brush, Figure 1.
189 The brush is formed by strong (quenched) polyelectrolytes

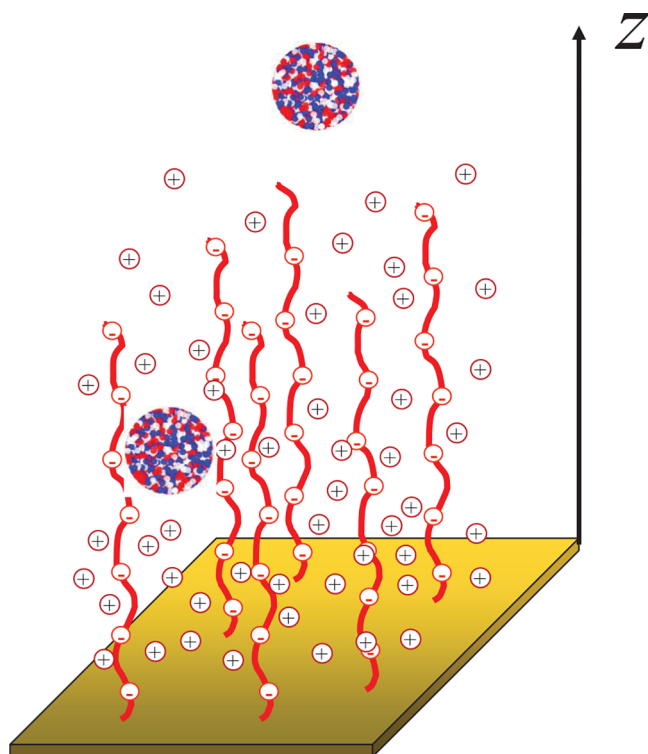


Figure 1. Schematics of an amphoteric NP insertion into a polyelectrolyte brush. Blue, red, and white areas on the globule surface correspond to cationic, anionic, and neutral residues, respectively.

190 (polyacids) with degree of polymerization $N \gg 1$ end-
191 tethered to the surface with density $\sigma = a^2/s$ (a is length of
192 monomer unit and s is the grafting area per chain). The PE
193 chains are assumed to be intrinsically flexible (with Kuhn
194 segment length on the order of monomer unit length, a), and
195 have a fraction α of (negatively) charged monomer units.

196 The pH in the solution (in the buffer) is fixed to the value of
197 pH_b . The solution contains monovalent (positively and
198 negatively charged) mobile ions of low molecular weight salt
199 with concentration (number density)

$$c_{b+} = c_{b-} = c_s \quad (2)$$

that controls the Debye screening length

$$\kappa^{-1} = (8\pi l_B c_s)^{-1/2} \quad (3)$$

Here, $l_B = e^2/\epsilon k_B T$ is the Bjerrum length (e is the elementary
charge, ϵ is the dielectric permittivity of the solvent, k_B is the
Boltzmann constant, and T is the temperature). In the
following we assume that $l_B = a$, which leads to the
proportionality factor ≈ 5 between molar concentration and
volume fraction $C_s = c_s a^3$ of the salt ions.

Because of excess electrostatic potential $\Psi(z) \leq 0$ created by
PE brush at distance z from the grafting surface (with the
reference value $\Psi(z = \infty) = 0$), and respective gradient in the
local concentration of hydrogen ions, the replacement of the
NP from buffer solution into PE brush at distance z is
accompanied by reionization of its cationic and anionic groups,
and leads to the concomitant change in the NP free energy,

$$\Delta F(z) = \Delta F_{\text{ion}}(z) + \Delta F_{\text{vol}}(z) \quad (4)$$

Here, $\Delta F_{\text{ion}}(z)$ and $\Delta F_{\text{vol}}(z)$ account for reionization free
energy and for the work against excess osmotic pressure inside
the brush, respectively.

2.2. Electrostatic Potential of a Quenched Polyelectrolyte Brush. The reduced self-consistent electrostatic
potential, $\psi(z) \equiv e\Psi(z)/k_B T$, in a negatively charged (anionic)
PE brush can be presented as

$$\psi_{\text{in}}(z) = \frac{z^2 - H^2}{H_0^2} + \psi_{\text{in}}(H), \quad 0 \leq z \leq H \quad (5)$$

Here, z is the distance from the grafting surface, H is the total
thickness of the brush (cutoff of the polymer density profile),
and H_0 is the characteristic length

$$H_0/a = \sqrt{\frac{8}{3\pi^2}} N\alpha^{1/2} \quad (6)$$

The value of constant $\psi_{\text{in}}(H)$ depends on the potential
calibration, and ensures continuity of the potential at the brush
edge, $\psi_{\text{in}}(H) = \psi_{\text{out}}(H)$. The potential outside the brush,
 $\psi_{\text{out}}(z)$, coincides with that of a uniformly charged plane with
the surface charge per unit area equal to the residual (negative)
charge per unit area of the brush

$$\tilde{q} = \int_0^H \rho(z) dz = -\frac{H}{2\pi l_B H_0^2} \quad (7)$$

with the residual charge density $\rho(z)$ specified by the Poisson
equation,

$$\frac{d^2 \psi_{\text{in}}(z)}{dz^2} = -4\pi l_B \rho(z) \quad (8)$$

(Here and below, charge is measured in the elementary charge,
 e , units.) The electrostatic potential outside the brush is thus
formulated as³⁰

$$\psi_{\text{out}}(z) = -2 \ln \left[\frac{(\kappa \tilde{\Lambda} + \sqrt{(\kappa \tilde{\Lambda})^2 + 1} - 1) + (\kappa \tilde{\Lambda} - \sqrt{(\kappa \tilde{\Lambda})^2 + 1} + 1) e^{-\kappa(z-H)}}{(\kappa \tilde{\Lambda} + \sqrt{(\kappa \tilde{\Lambda})^2 + 1} - 1) - (\kappa \tilde{\Lambda} - \sqrt{(\kappa \tilde{\Lambda})^2 + 1} + 1) e^{-\kappa(z-H)}} \right] \quad (9)$$

with the Gouy–Chapman length

$$\tilde{\Lambda} = \frac{1}{2\pi l_B |\bar{q}|} = \frac{H_0^2}{H} \quad (10)$$

The latter controls distributions of the electrostatic potential and small mobile ions outside the brush, i.e., at $z \geq H$. The potential defined by eq 9 vanishes at $z \rightarrow \infty$. The cutoff of the polymer density profile, $z = H$, is found from the condition of conservation of number of monomer units in grafted chains. The minimal value reached by the electrostatic potential at the grafting surface, $z = 0$,

$$\psi_{in}(0) = -\frac{H^2}{H_0^2} + \psi(H) = -\frac{H^2}{H_0^2} + 2 \ln \left[\frac{\sqrt{(\kappa \tilde{\Lambda})^2 + 1} - 1}{\kappa \tilde{\Lambda}} \right] \quad (11)$$

is the increasing function of salt concentration c_s in the buffer but the decreasing function of the grafting density σ . However, the potential difference across the brush,

$$-\psi_{in}(0) + \psi(H) = \frac{H^2}{H_0^2} \quad (12)$$

decreases as a function of salt concentration and increases upon an increase in the grafting density, because the brush thickness H decreases as a function of salt concentration, but increases as a function of σ .

The polymerization degree N of the grafted PE chains weakly affects $\psi(0)$, while the brush thickness $H \sim N$. More detailed derivation and typical shapes of the electrostatic potential profile inside and outside the brush are presented in SI.

Notably, the parabolic shape of electrostatic potential $\psi_{in}(z)$ in eq 5 holds if the stretched brush-forming chains are still far from full extension (i.e., $H \leq L = aN$). An approach to full extension of the tethered PE chains ($H \rightarrow L$) modifies electrostatic potential $\psi_{in}(z)$ as³¹

$$\psi_{in}(z) = \frac{3}{\alpha} \ln \frac{\cos(\pi z/2L)}{\cos(\pi H/2L)}$$

Electrostatic potential $\psi_{out}(z)$ outside strongly stretched PE brush is given by eq 9 with renormalized Gouy–Chapman length

$$\tilde{\Lambda} = \frac{H_0^2}{H} \frac{(\pi H/2L)}{\tan(\pi H/2L)}$$

In the following we assume that the tethered PEs are moderately charged (with degree of ionization $\alpha < 1$) to ensure the parabolic shape of $\psi_{in}(z)$.

3. RESULTS AND DISCUSSION

3.1. Ionic Contribution to the Free Energy. Transfer of NP from the bulk of solution in PE brush is accompanied by the change in ionization states of both basic and acidic groups on NP surface. The ionic part of the differential free energy can be expressed as²⁸

$$\Delta F_{ion}(z)/k_B T = \sum_{i+} N_{i+} \ln \left(\frac{1 - \alpha_{i+}(z)}{1 - \alpha_{bi+}} \right) + \sum_{i-} N_{i-} \ln \left(\frac{1 - \alpha_{i-}(z)}{1 - \alpha_{bi-}} \right) \quad (13)$$

where α_{bi+} , $\alpha_{i+}(z)$, α_{bi-} , and $\alpha_{i-}(z)$ are the respective degrees of ionization of basic and acidic monomer units on the surface of NP placed at distance z from the grafting surface and in the bulk of the solution (at $z = \infty$).

Here,

$$\alpha_{i+}(z) = (1 + K_{i+}/[H^+(z)])^{-1} \equiv (1 + 10^{\text{pH}(z) - \text{p}K_{i+}})^{-1} \\ = \left(1 + \frac{1 - \alpha_{bi+}}{\alpha_{bi+}} \exp(\psi(z)) \right)^{-1} \quad (14)$$

and

$$\alpha_{i-}(z) = (1 + [H^+(z)]/K_{i-})^{-1} \\ \equiv (1 + 10^{\text{p}K_{i-} - \text{pH}(z)})^{-1} \\ = \left(1 + \frac{1 - \alpha_{bi-}}{\alpha_{bi-}} \exp(-\psi(z)) \right)^{-1} \quad (15)$$

The respective degrees of ionization of ionogenic groups $i\pm$ in the buffer are

$$\alpha_{bi+} = (1 + K_{i+}/[H^+]_b)^{-1} = (1 + 10^{\text{p}H_b - \text{p}K_{i+}})^{-1} \quad (16)$$

and

$$\alpha_{bi-} = (1 + [H^+]_b/K_{i-})^{-1} = (1 + 10^{\text{p}K_{i-} - \text{p}H_b})^{-1} \quad (17)$$

$[H^+(z)]$ is the local concentration of hydrogen ions (specifying local $\text{pH}(z) = -\log[H^+(z)]$), $\text{pH}_b \equiv \text{pH}(z = \infty) = -\log[H^+(z = \infty)]$, and K_{i+} and K_{i-} are respective acidic ionization constants of basic and acidic groups.

According to eqs 14 and 15, ionization of acidic and basic ionogenic groups is controlled by local electrostatic potential $\psi(z)$ in the brush, while the Coulomb interactions between ionized groups on NP surface are disregarded. These interactions could shift the ionization constants with respect to “bare” constants K_{i+} and K_{i-} (see refs 35 and 36). Within the applied here approximation, $\{N_{i\pm}\}$ and $\{K_{i\pm}\}$ are considered as independent sets of variables. We also neglect the electrostatic potential gradient on the length scale of NP spatial dimensions.

The spacial distribution of hydrogen ions can be expressed as

$$[H^+(z)] = [H^+]_b \exp(-\psi(z)) \quad (18)$$

As long as hydrogen ions are distributed between PE brush and solution according to eq 18, lower electrostatic potential inside the brush, $\Psi(z) \leq 0$, indicates that local concentration of H^+ ions inside the brush is larger than in the bulk of the solution. As a result, the degree of ionization of basic residues inside polyanionic brush is higher, while the degree of ionization of acidic residues is lower than in the bulk of the solution (eqs 14 and 15). The sign of $\Delta F_{ion}(z)$ is determined by the balance between reionization free energies of basic and acidic monomer units (the first and the second terms in eq 13, respectively).

The net charge on NP (measured in the elementary charge units e) depends on its position z with respect to the grafting surface and can be expressed as

$$Q(z) = \sum_{i+} N_{i+} \alpha_{i+}(z) - \sum_{i-} N_{i-} \alpha_{i-}(z) \quad (19)$$

while the NP charge in the buffer is given by

$$Q_b = Q(z = \infty) = \sum_{i+} N_{i+} \alpha_{bi+} - \sum_{i-} N_{i-} \alpha_{bi-} \quad (20)$$

The isoelectric point, pH_{IEP} , corresponds to pH_b at which the NP charge in the buffer vanishes, $Q_b = 0$.

We focus primarily on the case of $\text{pH}_b \geq \text{pH}_{IEP}$, that is, when the NP in the bulk of the solution is charged negatively,

336 $Q_b \leq 0$, i.e., similarly to the brush. Because the electrostatic
 337 potential $\psi(z)$ created by the brush is a monotonically
 338 increasing function of z (i.e., monotonically increasing in
 339 absolute value upon approaching the grafting surface), the net
 340 charge of the NP $Q(z)$ monotonically increases upon
 341 approaching the grafting surface and, depending on the sets
 342 of parameters $\{N_{i\pm}, K_{i\pm}\}$, $\{c_s, \text{pH}_b\}$, $\{\alpha, N, \sigma\}$, may remain
 343 negative or invert its sign to positive at some particular
 344 distance z^* from the grafting surface, so that

$$Q(z = z^*) = 0$$

345 Remarkably, z^* may correspond to the NP position either
 346 inside, or outside the brush (close to its edge). The position z^*
 347 can be found from the equation

$$348 \psi(z^*) = -\Delta\text{pH}_b / \log_{10} e \approx -2.3\Delta\text{pH}_b \quad (21)$$

349 with

$$\Delta\text{pH}_b = \text{pH}_b - \text{pH}_{\text{IEP}}$$

350 which implies (with the account of eq 18) that local
 351 $\text{pH}(z = z^*)$ at $z = z^*$ coincides with pH_{IEP} for NP in solution.
 352 Using eqs 13 and 19, one can demonstrate that

$$353 \left(\frac{\partial \Delta F_{\text{ion}}(z)}{\partial z} \right)_{z^*} = 0 \quad (22)$$

354 that is, the ionization free energy passes through a maximum at
 355 $z = z^*$, i.e., in the point of the charge inversion. Indeed,

$$\frac{\partial \Delta F_{\text{ion}}(z)}{\partial z} = \frac{\partial \Delta F_{\text{ion}}}{\partial \lambda} \cdot \frac{\partial \lambda(z)}{\partial z}$$

356 where $\lambda(z) \equiv \exp(\psi(z))$. By taking the derivative of the r.h.s.
 357 of eq 13 with respect to $\lambda(z)$ (with the account of eqs 14 and
 358 15), one arrives at

$$359 \frac{\partial \Delta F_{\text{ion}}(z)}{\partial z} = \frac{1}{\lambda} \frac{\partial \lambda(z)}{\partial z} \cdot Q(z) = \frac{\partial \psi(z)}{\partial z} \cdot Q(z) \quad (23)$$

360 where the position-dependent charge $Q(z)$ of NP is given by
 361 eq 19. As soon as $\lambda(z)$ is a positive, monotonously increasing
 362 function of z in the whole range of $z \in [0, \infty)$, eq 23 indicates
 363 that $\Delta F_{\text{ion}}(z)$ exhibits a maximum in the NP charge inversion
 364 point, $z = z^*$.

365 When $\Delta F_{\text{ion}}(z = 0) \leq 0$ and $z^* \geq 0$, absorption of NP by the
 366 brush is thermodynamically favorable, and the minimum in
 367 $\Delta F_{\text{ion}}(z)$ (reached at the grafting surface, $z = 0$) is separated
 368 from the exterior solution by the potential barrier with the
 369 height $\Delta F_{\text{ion}}(z^*)$ located at $z = z^*$. As we demonstrate below,
 370 the charge inversion may occur at $z = z^* \geq 0$ even when
 371 $\Delta F_{\text{ion}}(z = 0) \geq 0$. In this case, the localization of positively
 372 charged NP inside polyanionic brush corresponds to a
 373 metastable state. Finally, when z^* decreases down to zero,
 374 the charge inversion inside the brush does not take place and
 375 the insertion free energy $\Delta F_{\text{ion}}(z)$ becomes a monotonically
 376 decreasing function of z . As a result, the Coulomb force pushes
 377 NP out of the brush and no absorption of NPs by PE brush
 378 occurs spontaneously.

379 Obviously, if NP is charged positively in the solution,
 380 $Q_b \geq 0$, then $\Delta F_{\text{ion}}(z) \leq 0$ at $\forall z \in [0, \infty)$ and is a
 381 monotonically increasing function,
 382 $\partial \Delta F_{\text{ion}}(z) / \partial z \geq 0 \forall z \in [0, \infty)$.

383 **3.2. Osmotic Contribution to the Free Energy.** The
 384 second term in eq 4 accounts for the work against excess

osmotic pressure of mobile ions inside the brush and in the 385
 double electrical layer outside. If the concentrations of mobile 386
 monovalent ions of low molecular weight salt in the buffer (at 387
 $z = \infty$) are $c_{b+} = c_{b-} = c_s$, then their concentrations at arbitrary 388
 distance z from the grafting surface are given by the Boltzmann 389
 law, 390

$$c_{\pm}(z) = c_s \exp(\mp\psi(z)) \quad (24) \quad 391$$

and the excess osmotic pressure is 392

$$\Pi(z)/k_B T = c_+(z) + c_-(z) - 2c_s = \quad (25) \quad 393$$

$$c_s (\exp(\psi(z)/2) - \exp(-\psi(z)/2))^2 = 4c_s \sinh^2(\psi(z)/2) \quad (26) \quad 394$$

Hence, the osmotic contribution to the insertion free energy, 395

$$\Delta F_{\text{vol}}(z)/k_B T = 4Vc_s \sinh^2(\psi(z)/2) \quad (27) \quad 396$$

is proportional to NP volume V and monotonically decreases 397
 with z . Hence, the derivative of this second term in the free 398
 energy in eq 4 always provides a thermodynamic force 399
 expelling the NP from the brush. 400

We remark that in sufficiently dense or/and weakly charged 401
 brushes the nonelectrostatic (excluded volume) interactions 402
 provide the dominant contribution to the osmotic pres- 403
 sure.^{37–39} However, in the present work we focus at sufficiently 404
 strongly charged brushes in which the electrostatic interactions 405
 dominate over the short-range repulsions between monomer 406
 units. 407

3.3. NP with Two Types of Ionizable Sites. Below we 408
 focus on a particular case when the NP comprises one type of 409
 cationic groups with ionization constant K_+ and one type of 410
 anionic groups with the ionization constant K_- . This 411
 simplification allows us to analyze the main trends in NP 412
 interaction with PE brush at variable environmental conditions 413
 (pH_b and c_s) and NP volume V . 414

The fraction of positively charged ionizable monomer units 415
 is defined as 416

$$f_+ = \frac{N_+}{N_- + N_+} \equiv \frac{N_+}{N_{\Sigma}} \quad (28) \quad 417$$

where $N_+ + N_- = N_{\Sigma}$ is the total number of ionizable (basic 418
 and acidic) groups, and the ionic contribution ΔF_{ion} in eq 13 419
 with $i_+ = i_- = 1$ reduces to 420

$$\Delta F_{\text{ion}}(z)/k_B T = N_{\Sigma} \left[f_+ \ln \left(\frac{1 - \alpha_+(z)}{1 - \alpha_{b+}} \right) + (1 - f_+) \ln \left(\frac{1 - \alpha_-(z)}{1 - \alpha_{b-}} \right) \right] \quad (29) \quad 421$$

In section 3.3.1, we start with the analysis of $\Delta F_{\text{ion}}(z)$, which 422
 is the dominant contribution to the overall free energy, 423
 $\Delta F(z) \approx \Delta F_{\text{ion}}(z)$, in the case of small NPs. In the following 424
 section 3.3.2 we consider the interplay between $\Delta F_{\text{ion}}(z)$ and 425
 $\Delta F_{\text{vol}}(z)$ which becomes essential for increasingly bulky 426
 charged species and may prevent NP absorption by PE 427
 brush even if the reionization free energy, ΔF_{ion} , provides a 428
 driving force for it. 429

3.3.1. Reionization Free Energy for NP Interacting with 430
Polyelectrolyte Brush. Below we present typical ionization free 431
 energy profiles $\Delta F_{\text{ion}}(z)$ normalized by the total number of 432
 ionizable sites N_{Σ} calculated for the NP with $f_+ = 0.5$ at varied 433
 pH_b , reduced salt concentration $C_s = c_s a^3$ and grafting density 434
 $\sigma = a^2/s$. We use model equal values of ionization constants 435
 $pK_- = pK_+ = 5$ that assures maximal impact of the reionization 436

437 free energy to the overall insertion free energy balance and
 438 corresponds at $f_+ = 0.5$ to the IEP $\text{pH}_{\text{IEP}} = 5$. In real experiment
 439 chosen parameters are sufficiently close to the pK_- value for
 440 carboxylic groups and not far from pK_+ value for, e.g.,
 441 $\text{N}(\text{CH}_3)_2$ groups.

442 The degree of polymerization of the brush-forming chains
 443 $N = 300$. Notably, C_s and σ affect the magnitude of the excess
 444 electrostatic potential created by the brush, whereas pH_b
 445 controls degrees of ionization of the cationic and anionic
 446 residues and the net charge of the globule Q_b in the buffer.

447 In Figure 2a,b, the position-dependent free energy $\Delta F_{\text{ion}}(z)$
 448 and charge $Q(z)$ are plotted as a function of distance z from

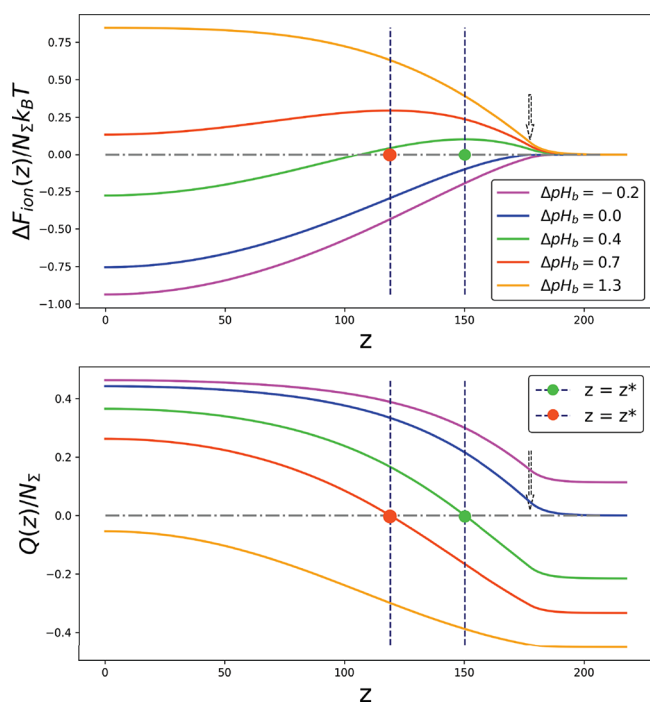


Figure 2. Position-dependent insertion free energy $\Delta F_{\text{ion}}(z)$ (a) and the NP charge $Q(z)$ (b) both normalized by N_Σ , as a function of the distance z from the grafting surface for a series of pH_b values around the IEP at fixed salt concentration $C_s = 10^{-3}$. Arrows indicate the upper boundary of the brush. Dashed vertical lines indicate the charge inversion point, $z = z^*$. Dashdot horizontal lines indicate $\Delta F_{\text{ion}}(z) = 0$ and $Q(z) = 0$. Colored circles in panels (a) and (b) correspond to the charge inversion points $z = z^*$.

449 the grafting surface for a series of pH_b values at constant salt
 450 concentration $C_s = 10^{-3}$.

451 In Figure 3a,b, we show cross sections of 2D profiles of the
 452 insertion free energy $\Delta F_{\text{ion}}(z, \Delta\text{pH}_b)$, and net charge
 453 $Q(z, \Delta\text{pH}_b)$ of the NP plotted at three selected values of
 454 salt concentration C_s .

455 As one can see from Figures 2b and 3b and follows from eq
 456 19, because of reionization of cationic and anionic sites in the
 457 electrostatic potential of the polyanionic brush, net charge
 458 $Q(z)$ of the NP is always a decreasing function of z .

459 Sufficiently far above the IEP (e.g., at $\Delta\text{pH}_b = 1.3$ in Figure
 460 2a,b), the NP is negatively charged in the buffer and remains
 461 negatively charged, $Q(z) \leq 0 \forall z \in [0, \infty)$, though $|Q(z)|$
 462 decreases in the absolute value upon insertion of the NP into
 463 the brush. The insertion free energy in this case is positive,
 464 $\Delta F_{\text{ion}}(z) > 0 \forall z \in [0, \infty)$, and monotonously decreasing

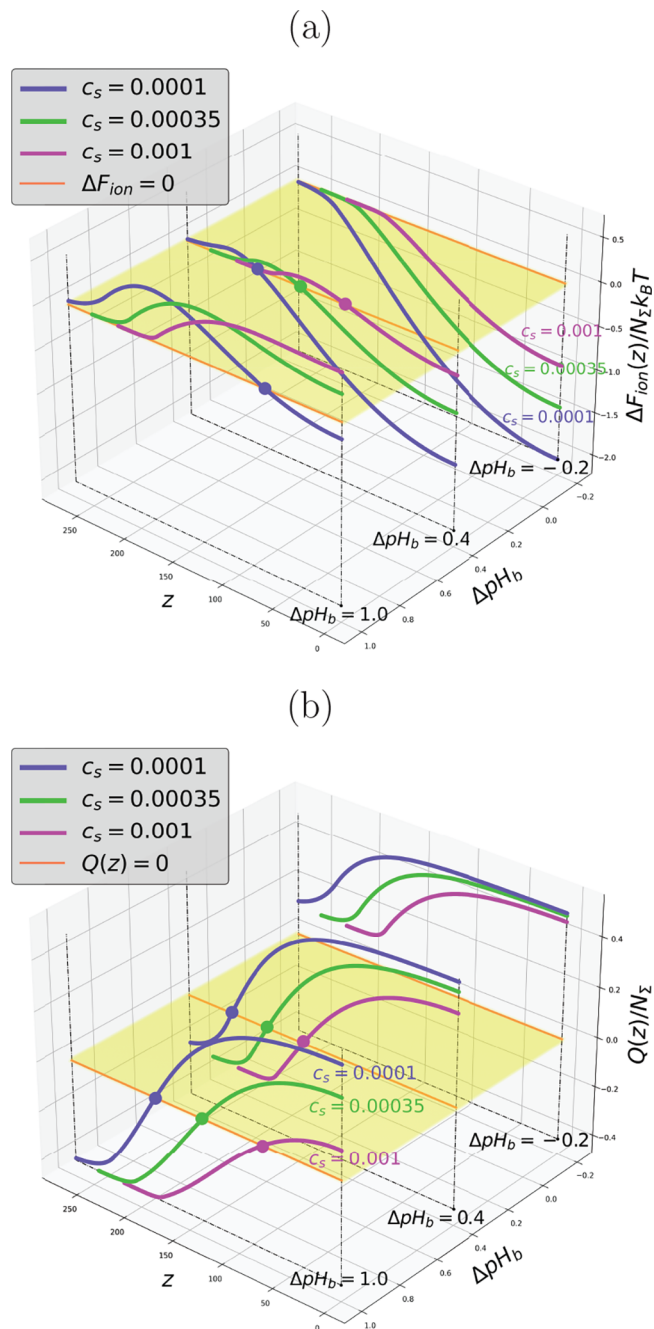


Figure 3. Cross sections of the 2D profiles of the insertion free energy $\Delta F_{\text{ion}}(z, \Delta\text{pH}_b)$ (a) and NP charge $Q(z, \Delta\text{pH}_b)$ (b), both normalized by N_Σ , for a set of values of salt concentration (with the corresponding color code, as indicated at the curves). Colored circles in panel (a) indicate points of vanishing free energy, $\Delta F_{\text{ion}}(z, \Delta\text{pH}_b) = 0$; colored circles in panel (b) correspond to the charge inversion points $z = z^*$.

function of z , $\partial\Delta F_{\text{ion}}(z)/\partial z \leq 0$, that is, the NP is expelled
 465 from the brush. 466

On the contrary, below the IEP, at $\Delta\text{pH}_b < 0$, the charge of
 467 the NP is positive, $Q(z) > 0 \forall z \in [0, \infty)$ (Figures 2b and 3b). 468
 The free energy $\Delta F_{\text{ion}}(z) < 0 \forall z \in [0, \infty)$ is negative and 469
 monotonously decreases upon approaching the grafting surface 470
 (Figures 2a and 3a). In this case, the NP and the brush are 471
 oppositely charged, and the NP is driven into the brush by the 472
 attractive Coulomb force. The depth of the free energy edge 473
 minimum at the grafting surface, $\Delta F_{\text{ion}}(z = 0)$, grows upon a 474

475 decrease in ΔpH_b , or upon an increase in the magnitude of the
 476 negative electrostatic potential at the surface which can be
 477 induced either by a decrease in salt concentration C_s (Figure
 478 S2a) or by an increase in grafting density σ (Figure S2b). The
 479 same applies also at the IEP, $pH = pH_{IEP}$, when the NP charge
 480 is vanishing far away from the brush, but becomes positive and
 481 monotonously increases when NP approaches and enters the
 482 brush.

483 The most peculiar patterns in $\Delta F_{ion}(z)$ and $Q(z)$ are
 484 observed at $\Delta pH_b \geq 0$, i.e., slightly above the IEP, as illustrated
 485 by Figure 2a,b and the cross-section of the $\Delta F_{ion}(z, \Delta pH_b)$
 486 surface at $\Delta pH_b = 0.4$ in Figure 3a,b. In this case NP is charged
 487 negatively in the buffer, $Q_b < 0$, but inverts the sign of its
 488 charge upon embedding into the brush at $z = z^*$. That is, the
 489 NP charge $Q(z \geq z^*) \leq 0$ and $Q(z \leq z^*) \geq 0$. As
 490 demonstrated above, the free energy $\Delta F_{ion}(z)$ passes through a
 491 maximum in the charge inversion point $z = z^*$, i.e., $\Delta F_{ion}(z)$ is
 492 an increasing function of z at $z \in [0, z^*]$ and a decreasing
 493 function of z at $z \in [z^*, \infty)$. Obviously, $z^* \rightarrow \infty$ at $pH_b \rightarrow$
 494 pH_{IEP} .

495 In Figure 4 we present a typical zoomed profile of the free
 496 energy $\Delta F_{ion}(z)$ with maximum, corresponding to the $Q(z)$

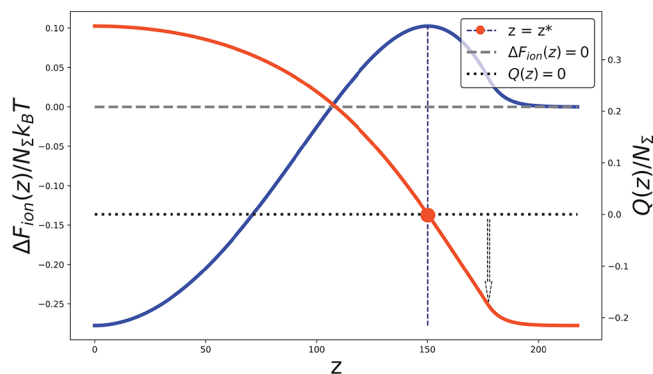


Figure 4. Characteristic dependence of the $\Delta F_{ion}(z)$ with a maximum at $z = z^*$ and corresponding dependence $Q(z)$ with charge inversion at $z = z^*$ plotted for $\Delta pH_b = 0.4$ both normalized by N_Σ . Salt concentration is $C_s = 10^{-3}$, grafting area per chain is $s/a^2 = 100$. Arrow indicate the upper boundary of the brush ($z = H$), and the charge inversion point $z = z^*$ is indicated by vertical dashed line and a red circle.

497 sign inversion point, and $\Delta F_{ion}(z = 0) < 0$. This free energy
 498 profile indicates the presence of electrostatic driving force for
 499 NP absorption by PE brush.

500 Remarkably, similar patterns in the position-dependent net
 501 charge were observed in Molecular Dynamic simulations²⁷ of
 502 ampholytic oligopeptide interacting with strongly charged
 503 starlike polyelectrolyte: in the vicinity of the IEP the
 504 oligopeptide charge inversion was observed upon approaching
 505 the center of the star. However, quantitative comparison of our
 506 results to those presented in ref²⁷ is challenging because of
 507 essentially different spatial distribution of polymer density and
 508 electrostatic field in a planar PE brush and in a single PE star.
 509 As seen in Figure 3a,b, an increase in salt concentration (at a
 510 given ΔpH_b) leads to the shift in the charge inversion point z^*
 511 toward the grafting surface, the decrease in $Q(z)$, and
 512 narrowing of the presurface potential well which simulta-
 513 neously becomes more shallow.

514 Upon a moderate increase in pH_b above the IEP, i.e., upon a
 515 decrease in the NP charge $Q_b < 0$ in the buffer, the charge

inversion point z^* is shifted toward the grafting surface, the
 magnitude of the maximum in $\Delta F_{ion}(z)|_{z=z^*}$ increases, and the
 depth of the presurface potential well, $|\Delta F_{ion}(z = 0)|$, decreases.
 In this regime, absorption of NPs by the brush remains
 thermodynamically favorable, but requires overcoming of the
 potential barrier with maximum at $z = z^*$. At sufficiently large
 number of ionizable groups on NP surface, $N_\Sigma \sim 10^2$, the
 barrier may increase up to $\sim 10k_B T$ thus completely hindering
 NP absorption by PE brush kinetically.

When ΔpH_b exceeds the threshold value $\Delta pH_b^{(abs)} \geq 0$ (that
 is, pH_b exceeds $pH_b^{(abs)} > pH_{IEP}$), the free energy $\Delta F_{ion}(z)$
 becomes positive at $\forall z \in [0, \infty)$. The free energy minimum at
 $z = 0$ remains separated from the bulk of the solution by the
 potential barrier located at $z = z^*$. Hence, the NP location
 inside the brush at $0 \leq z \leq z^*$ corresponds to a metastable
 state although the globule possesses positive net charge,
 $Q(z \leq z^*) \geq 0$ (see, e.g., the curves corresponding to
 $\Delta pH_b = 0.7$ in Figure 2a,b). Indeed, the local free energy
 minimum at $z = 0$ is separated from the global free energy
 minimum $\Delta F_{ion}(z = \infty) = 0$ by a potential barrier at $z = z^*$,
 which implies that, by definition,⁴⁰ the position of the NP in
 the brush corresponds not to an equilibrium, but to a
 metastable state.

Further increase in pH_b results in simultaneous increase in
 the magnitude of the potential barrier at $z = z^*$ and its
 displacement toward the grafting surface and concomitant
 decrease in the depth and width of the potential well.
 Eventually, $z^* \rightarrow 0$, and the free energy $\Delta F_{ion}(z)$ becomes a
 positive and monotonously decreasing function of z , so that
 the NP–PE brush interaction becomes purely repulsive.

Because the position-dependent net charge $Q(z)$ and the
 free energy $\Delta F_{ion}(z)$ depend on the brush local electrostatic
 potential $\psi(z)$, both properties are strongly affected by salt
 concentration in the buffer. The magnitude of $\psi(z)$ decreases,
 and its range shrinks as the salt concentration in the buffer
 increases (see Figure S2a in the Supporting Information).
 Therefore, the equilibrium absorption threshold can be crossed
 also by an increase in the salt concentration at constant pH_b , as
 demonstrated by series of the cross sections of the
 $\Delta F_{ion}(z, \Delta pH_b)$ surfaces corresponding to $\Delta pH_b = 1.0$ and
 different values of C_s in Figure 3a,b. For given set of parameters
 $\{f_+, K_+, K_-\}$ the defined above threshold $pH_b^{(abs)}$ depends on
 salt concentration C_s , as demonstrated in Figure 5.

In Figure 6a,b, we present $\Delta F_{ion}(z)$ and $Q(z)$ profiles for a
 number of selected salt concentrations C_s and constant
 $\Delta pH_b = 0.3$. In Figure 7a,b, we show cross sections of 2D
 profiles of the insertion free energy $\Delta F_{ion}(z, c_s)$, and net charge
 $Q(z, c_s)$ of the NP plotted at three selected values of ΔpH_b
 above the IEP. The values of pH_b are chosen sufficiently close
 to pH_{IEP} so that, at low salt concentration, $C_s = 10^{-3}$, the
 $\Delta F_{ion}(z)$ exhibits pronounced maxima at the charge inversion
 points and the edge minima at $z = 0$.

An increase in salt concentration leads to weakening of the
 electrical field created by PE brush, and the magnitude of the
 electrostatic potential $|\psi(z = 0)|$ decreases. Upon an increase in
 salt concentration, the charge inversion point $z = z^*$ is shifted
 to a smaller z , the free energy at the grafting surface,
 $\Delta F_{ion}(z = 0)$, increases, changes its sign from negative to
 positive, and $\Delta F_{ion}(z)$ acquires a monotonously decreasing
 shape corresponding to expulsion of NPs from PE brush. The
 larger the ΔpH_b , the smaller the salt concentration is needed to
 suppress charge inversion and eliminate the potential well at
 the grafting surface.

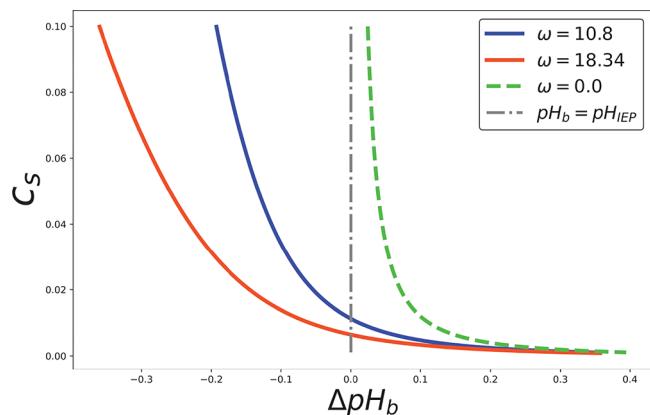


Figure 5. Dependences of salt concentration $C_s^{(\max)}$ corresponding to inversion of sign of $\Delta F_{\text{ion}}(z=0)$ (dashed line) and $C_s^{(\max, \omega)}$ corresponding to inversion of sign of $\Delta F_{\text{ion}}(z=0) + \Delta F_{\text{vol}}(z=0)$ (solid lines) for selected values of ω (see color code in the figure) on deviation ΔpH_b from the IEP.

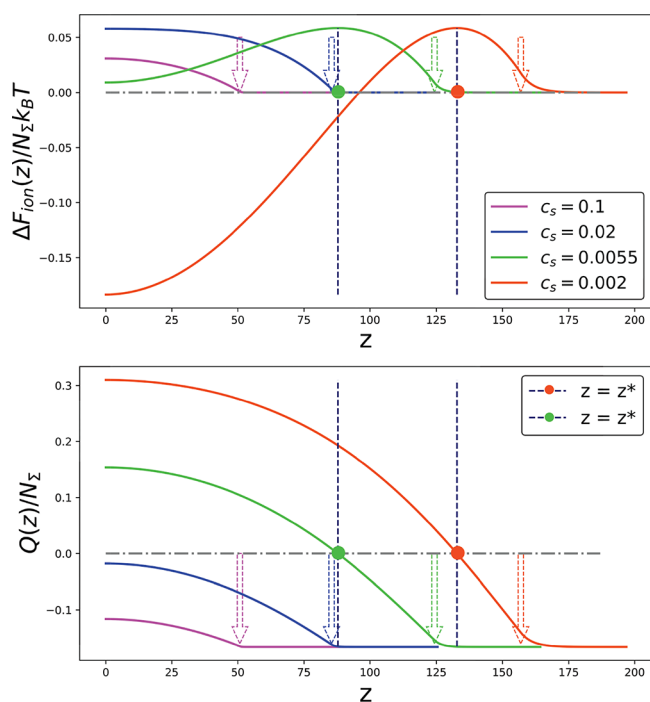


Figure 6. Position-dependent insertion free energy $\Delta F_{\text{ion}}(z)$ (a) and the NP charge $Q(z)$ (b), both normalized by N_Σ , as a function of the distance z from the grafting surface for a series of salt concentration C_s values at $\Delta \text{pH}_b = 0.3$. Arrows indicate the salt-dependent position of the upper boundary of the brush. Dashed vertical lines indicate the charge inversion points, $z = z^*$. Dashdot horizontal lines indicate $\Delta F_{\text{ion}}(z) = 0$ and $Q(z) = 0$. Colored circles in panels (a) and (b) correspond to the charge inversion points $z = z^*$.

579 Remarkably, if $\Delta \text{pH}_b > 0$ and $Q|_{z=0} < 0$ or, on the contrary,
 580 $\Delta \text{pH}_b < 0$ and $Q|_{z=0} > 0$, the addition of salt does not lead to
 581 qualitative changes in the shape of the $\Delta F_{\text{ion}}(z)$ curves: They
 582 are monotonously decreasing or monotonically increasing in
 583 the former and in the latter case, respectively, but their
 584 magnitudes (the height of the potential barrier or the depth of the
 585 potential well) as well as the range of the potential
 586 (proportional to the brush thickness H) decrease.

587 The effect of the grafting density $\sigma = a^2/s$ on the $\Delta F_{\text{ion}}(z)$
 588 curves is illustrated by Figure 8: An increase in the grafting

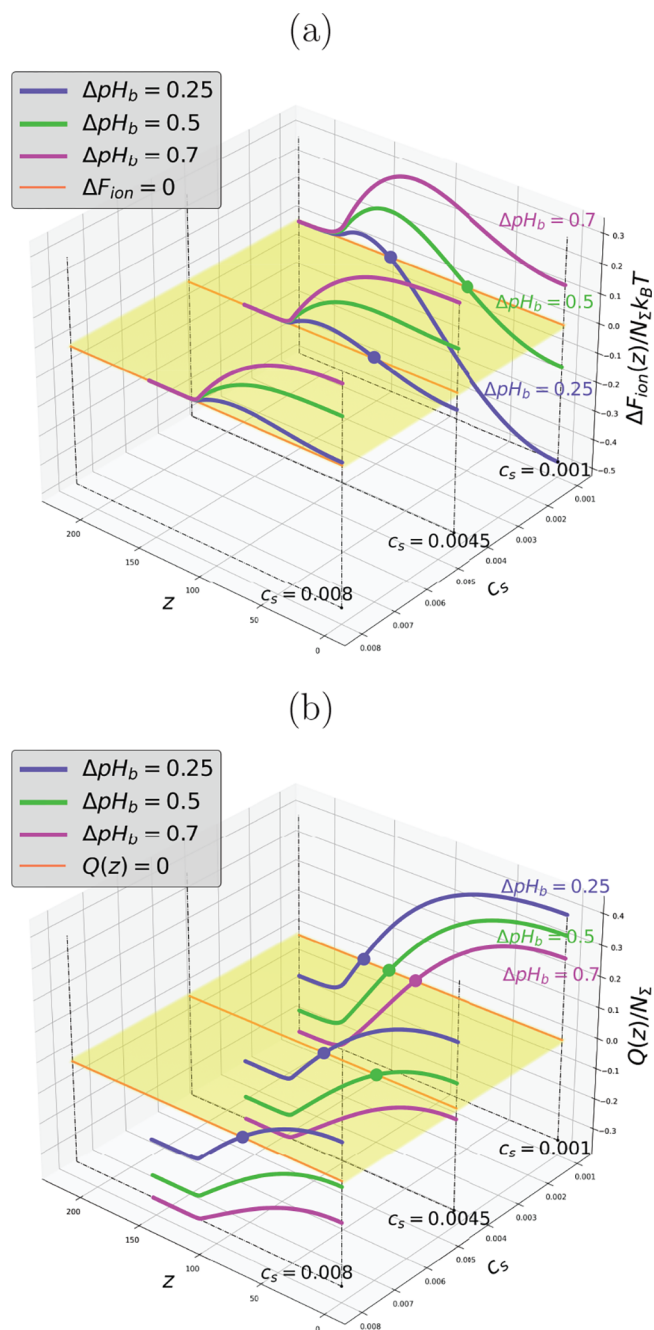


Figure 7. Cross sections of the 2D profiles of the insertion free energy $\Delta F_{\text{ion}}(z, c_s)$ (a) and NP charge $Q(z, c_s)$ (b), both normalized by N_Σ , for a set of values of pH_b (with the corresponding color code, as indicated at the curves). Colored circles in panel (a) indicate points of vanishing free energy, $\Delta F_{\text{ion}}(z, \Delta \text{pH}_b) = 0$; colored circles in panel (b) correspond to the charge inversion points $z = z^*$.

density enhances electrostatic potential, causes additional
 589 stretching of the brush-forming PE chains (an increase in the
 590 brush thickness H) and might drive NP absorption into
 591 sufficiently dense PE brush. 592

3.3.2. *Interplay between NP Charge and Volume.* For an
 593 ampholytic NP (protein globule) the ionic contribution to the
 594 insertion free energy $\Delta F_{\text{ion}}(z)$ is complemented by the osmotic
 595 term $\Delta F_{\text{vol}}(z)$. In this subsection we unravel the competitive
 596 effects of the electrostatic (attractive) and osmotic (repulsive)
 597 forces on NP absorption by PE brush. 598

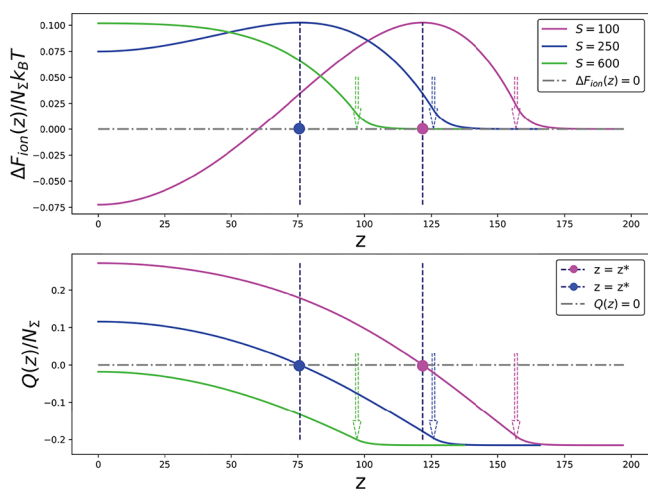


Figure 8. Position-dependent insertion free energy $\Delta F_{\text{ion}}(z)$ (a) and the NP charge $Q(z)$ (b) both normalized by N_{Σ} , as a function of the distance z from the grafting surface for a series of $s = a^2/\sigma$ values at $C_s = 10^{-3}$, $\Delta \text{pH}_b = 0.4$ (with the corresponding color code, as indicated at the curves). Arrows indicate the upper boundary of the brush. Dashed vertical lines indicate the charge inversion point, $z = z^*$. Dashdot horizontal lines indicate $\Delta F_{\text{ion}}(z) = 0$ and $Q(z) = 0$. Colored circles in panels (a) and (b) correspond to the charge inversion points $z = z^*$.

Table 1. Proteins Corresponding to the ω Coefficient

ω	name of the protein
2.0	human serum albumin
3.2	Des-Phe B1 bovine insulin
3.5	phospholipase A2 (PLA2) from <i>Naja naja</i> venom
3.7	α -lactalbumin
4.9	human interleukin-6
5.3	human hemoglobin A2
6.1	human sex hormone-binding globulin
7.5	interleukin-37
8.6	bovine β -lactoglobulin
10.3	bromoperoxidase A1
15.7	human interleukin-17A
29.2	pumpkin seed globulin

For given globule volume V , $\Delta F_{\text{vol}}(z)$ in eq 27 (as well as 628
 $|\psi(z)|$ in eqs 5 and 9) is a decreasing function of salt 629
concentration c_s in the buffer, and an increasing function of the 630
brush grafting density $\sigma = a^2/s$. 631

Consider first the scenario when $\Delta \text{pH}_b \geq 0$, and the 632
 $\Delta F_{\text{ion}}(z)$ curve exhibits a characteristic pattern with the 633
maximum at $z = z^*$ and the minimum at the grafting surface, 634
 $\Delta F_{\text{ion}}(z = 0) \leq 0$. In this case, the ionic interactions provide a 635
driving force for the globule absorption above IEP, 636
accompanied by the NP charge reversal. In Figure 9a we 637 638
illustrate the evolution of the insertion free energy profile, 639
 $\Delta F(z) = \Delta F_{\text{ion}}(z) + \Delta F_{\text{vol}}(z)$, upon an increase in the 640
parameter ω . As one can see in Figure 9a, at small values of ω 641
(NPs with relatively small volume V and large number N_{Σ} of 642
ionizable groups) the $\Delta F(z)$ curve has the same shape as 643
 $\Delta F_{\text{ion}}(z)$. That is, exhibits a maximum close to the edge of the 643

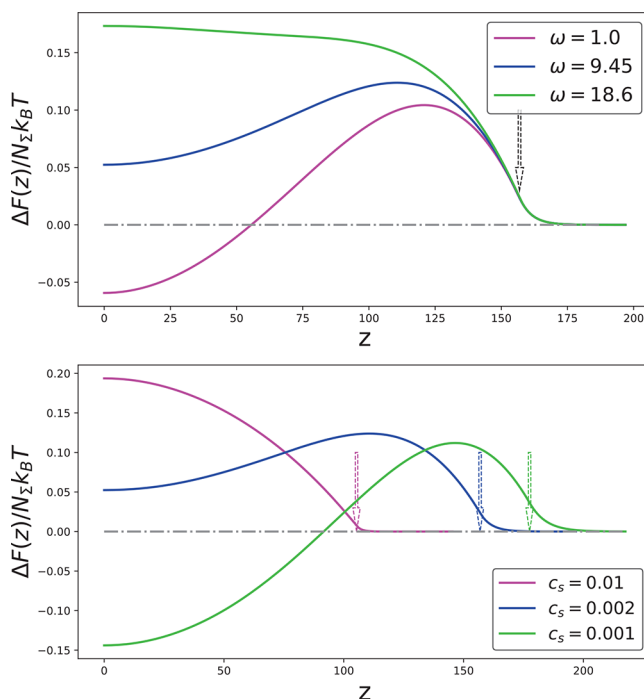


Figure 9. Total free energy curves $\Delta F(z) = \Delta F_{\text{ion}}(z) + \Delta F_{\text{vol}}(z)$ normalized by N_{Σ} corresponding to different globule volume to the number of charge ratio ω at $C_s = 0.002$ (a) and at fixed $\omega = 9.45$ and varied salt concentration C_s (b). Other parameters are $s/a^2 = 100$. The brush boundary, $z = H$, is indicated by the arrows. Dashdot horizontal lines indicate $\Delta F(z) = 0$.

599 While the ionic part of the insertion free energy, $\Delta F_{\text{ion}}(z)$,
600 may exhibit different patterns as a function of z , the osmotic
601 contribution $\Delta F_{\text{vol}}(z)$ given by eq 27 is always a positive and
602 monotonously decreasing function of z . As a result, at
603 $\Delta \text{pH}_b > 0$ and $\Delta F_{\text{ion}}(z) > 0$ at any $z \geq 0$, the net free energy
604 is positive, $\Delta F(z) = \Delta F_{\text{ion}}(z) + \Delta F_{\text{vol}}(z) > 0$ as well, and NP
605 absorption by PE brush is unfavorable. Even when the ionic
606 interactions provide a driving force for globule absorption, (i.e.,
607 $\Delta F_{\text{ion}}(z = 0) < 0$), the net insertion free energy $\Delta F(z = 0)$ may
608 be still positive due to the osmotic term, $\Delta F_{\text{vol}}(z = 0)$,
609 overcompensating the attractive ionic contribution.
610 Using eqs 4, 27, and 29, the NP insertion free energy can be
611 presented as

$$\Delta F(z) = N_{\Sigma} \left[f_+ \ln \left(\frac{1 - \alpha_+(z)}{1 - \alpha_{b+}} \right) + (1 - f_+) \ln \left(\frac{1 - \alpha_-(z)}{1 - \alpha_{b-}} \right) \right] + 4\omega C_s \sinh^2(\psi(z)/2) \quad (30)$$

612 where we have introduced the following parameter

$$\omega = V/a^3 N_{\Sigma} \quad (31)$$

615 which is equal to the average globule volume per ionizable
616 group. Because $\Delta F_{\text{ion}}(z) \sim N_{\Sigma}$ (eq 29) and $\Delta F_{\text{vol}}(z) \sim V$ (eq
617 27), the relative strength of the osmotic and ionic
618 contributions, $\Delta F_{\text{vol}}/\Delta F_{\text{ion}}$, depends on the parameter ω .
619 Remarkably, ω is an increasing function of the globule
620 dimensions (since N_{Σ} does not grow faster than the globule
621 surface area Σ).

622 In Table 1 we list approximate estimates of the parameter ω
623 for a number of globular proteins, using values of V and N_{Σ}
624 from the literature.⁴¹ Notably, the values of ω in Table 1
625 constitute lower boundaries, since all the ionizable residues
626 (not necessarily located at the globule surface) have been
627 accounted for in the corresponding protein.

644 brush and reaches a negative value at the grafting surface, but
 645 with the curve as a whole moving upward. Importantly,
 646 position of the maximum, $z = z_{\max}$ is shifted toward the
 647 grafting surface with respect to z^* ($z_{\max} \leq z^*$), and does not
 648 correspond anymore to the globule charge inversion threshold
 649 (i.e., $Q(z = z_{\max}) > 0$). Further increase in the globule volume
 650 V (i.e., an increase in ω) results in further shift of the
 651 maximum toward the grafting surface, and the increase in both,
 652 $\Delta F(z_{\max})$ and $\Delta F(z = 0)$. The latter becomes eventually
 653 positive indicating that the osmotic repulsion overcompensates
 654 the electrostatic attraction making globule absorption
 655 thermodynamically unfavorable. At large ω , $\Delta F(z)$ become a
 656 monotonously decreasing function of z with $\Delta F(z) > 0$ at any
 657 $z \geq 0$.

658 An increase in salt concentration leads to the simultaneous
 659 decrease in both, the electrostatic driving force for NP
 660 absorption and the osmotic repulsion, and eventually
 661 suppresses the globule absorption by PE brush (as seen in
 662 Figure 9b). The combined effects of the NP volume-to-charge
 663 ratio ω and salt concentration c_s are illustrated also by cross
 664 sections of the 2D profiles of the insertion free energy curves,
 665 $\Delta F(z, c_s)$ and $\Delta F(z, \omega)$, presented in Figure 10a and b,
 666 respectively. Remarkably, an increase in ω or/and in salt
 667 concentration c_s leads to the decrease in depth of the minimum
 668 in $\Delta F(z)$ (and, eventually, its disappearance), but does not
 669 affect its position at $z = 0$.

670 As it follows from our analysis, only small protein globules
 671 with large number of ionizable groups are efficiently absorbed
 672 by PE brushes at $\Delta pH_b \geq 0$, while bigger ones are not (unless
 673 other driving forces are involved).

674 We now examine the interplay between forces of electro-
 675 static attraction and osmotic repulsion in the case $\Delta pH_b \leq 0$,
 676 i.e., when $Q(z) \geq 0$ at any $z \geq 0$. The free energy profiles
 677 $\Delta F(z)$ corresponding to progressively increasing values of ω
 678 are presented in Figure 11a and Figure 12a. They demonstrate
 679 qualitatively new trends compared to the case $\Delta pH_b \geq 0$. For
 680 example, at $\omega = 15$ the ionic contribution to the free energy
 681 dominates, $\Delta F(z) \leq 0$ at any z , and thermodynamically most
 682 favorable position of the globule is close to the grafting surface.
 683 An increase in ω leads to the shift of the whole $\Delta F(z)$ curve
 684 upward and change in its shape: The repulsive osmotic
 685 contribution becomes dominant close to the grafting surface,
 686 so that $\Delta F(z = 0)$ becomes positive, and a potential well
 687 develops at the periphery of the brush where the negative ionic
 688 contribution $\Delta F_{\text{ion}}(z) < 0$ dominates over the osmotic
 689 repulsion. The width and the depth of the potential well
 690 decrease upon an increase in ω , and its position is shifted to
 691 the edge of the brush. Eventually, at large ω the peripheral
 692 potential well disappears, and $\Delta F(z)$ becomes a monotonously
 693 decreasing function of z , indicating expulsion of globules from
 694 PE brush.

695 Another trend is observed at $\Delta pH_b \leq 0$ if ω is small and
 696 kept constant, but the salt concentration increases, Figures 11b
 697 and 12b: Notably the magnitudes of both electrostatic
 698 (negative) and osmotic (positive) contributions to the free
 699 energy diminish upon an increase in salt concentration C_s . At
 700 very low salt concentration the electrostatic attraction
 701 dominates over osmotic repulsion at any distance from the
 702 surface and $\Delta F(z)$ is a monotonously increasing function of z .
 703 At higher salt concentrations, the osmotic (repulsive) part of
 704 the free energy starts to dominate in the proximal to the
 705 grafting surface region, while in the distal region ($z \approx H$) the
 706 electrostatic attraction, $\Delta F_{\text{ion}}(z)$, provides the dominant

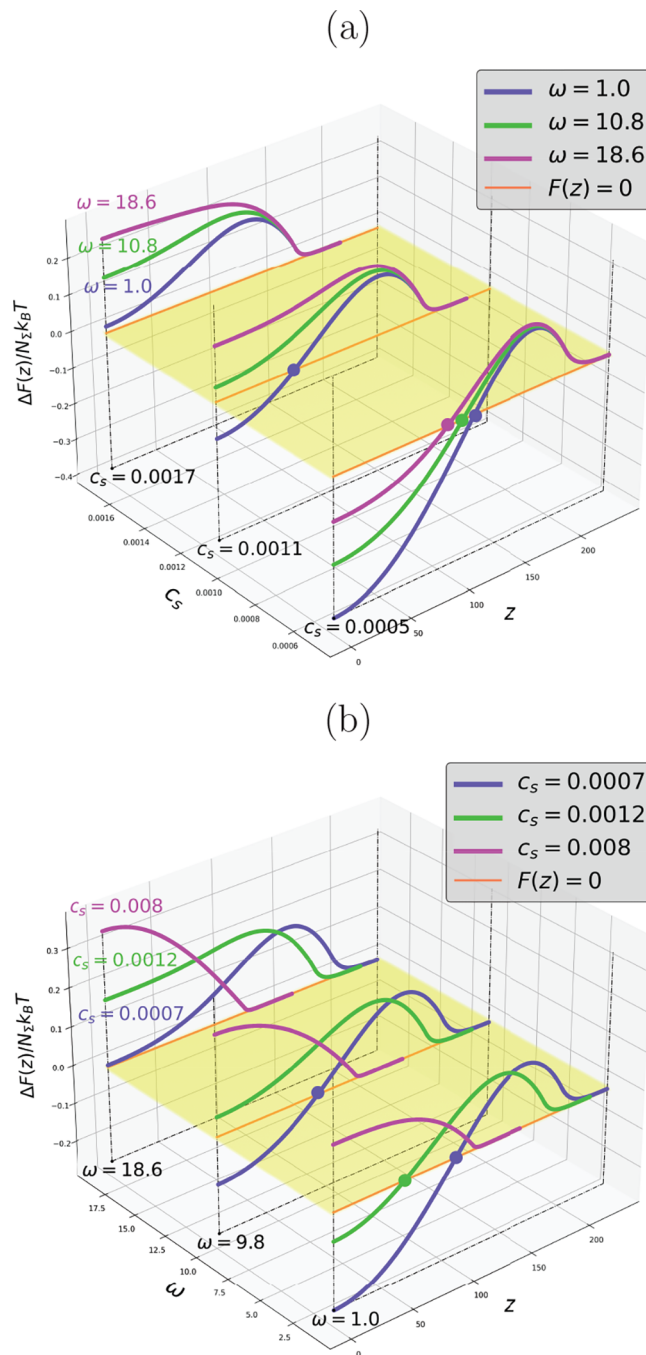


Figure 10. Cross sections of the 2D profiles of the total free energy curves $\Delta F(z, c_s) = \Delta F_{\text{ion}}(z, c_s) + \Delta F_{\text{vol}}(z, c_s)$ (a) and $\Delta F(z, \omega) = \Delta F_{\text{ion}}(z, \omega) + \Delta F_{\text{vol}}(z, \omega)$ (b), both normalized by N_s , for a set values of ω corresponding to different globule volume to the number of charges ratio (a) and different salt concentrations (b) (with the corresponding color code, as indicated at the curves). $s/a^2 = 100$. Colored circles in panels indicate points of vanishing free energy, $\Delta F(z, c_s) = 0$ and $\Delta F(z, \omega) = 0$.

contribution to $\Delta F(z)$. As a result, a minimum in $\Delta F(z)$ 707
 develops in the distal region. The depth of this minimum 708
 decreases and its position z_{\min} is shifted toward the grafting 709
 surface upon an increase in salt concentration and a 710
 concomitant decrease in the brush thickness H . Hence, when 711
 the osmotic contribution to the free energy becomes 712
 comparable to the ionic one due to sufficiently large globule 713
 volume or high salt concentration, the insertion free energy 714

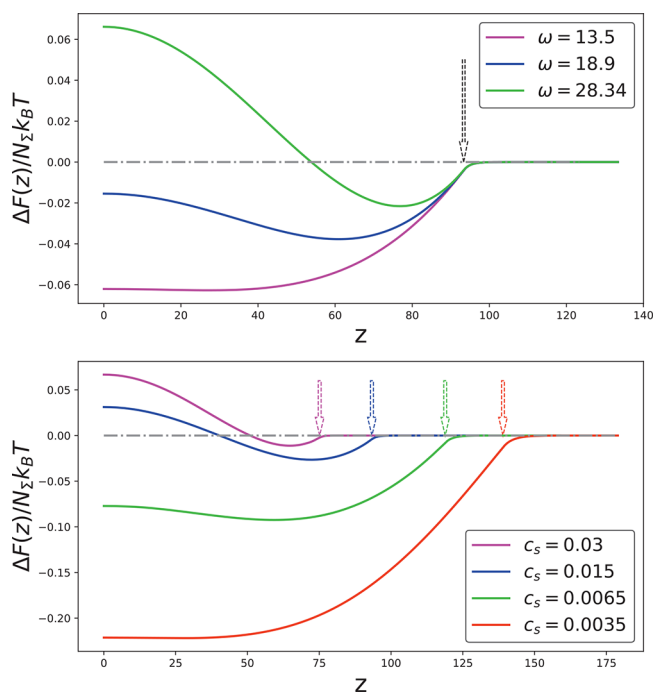


Figure 11. Total free energy curves $\Delta F(z) = \Delta F_{\text{ion}}(z) + \Delta F_{\text{vol}}(z)$ normalized by N_s , at different globule volume to the number of charges ratio ω . $c_s = 0.015$ (a) and at $\omega = 24.3$ and varied salt concentration (b). The brush boundary, $z = H$, is indicated by the arrows. Dashdot horizontal lines indicate $\Delta F(z) = 0$.

715 curves decrease from $\Delta F(z = 0) \geq 0$ in the proximal to the
 716 grafting surface region and pass through a minimum (with
 717 $\Delta F(z = z_{\text{min}}) \leq 0$) localized in the distal region of the brush.
 718 Solid lines in the diagram in Figure 5 correspond to the salt
 719 concentration $c_s^{(\text{max}, \omega)}$ separating regimes $\Delta F(0) \leq 0$
 720 (absorption) and $\Delta F(0) > 0$ (repulsion). As follows from
 721 Figure 5, this boundary is systematically displaced toward
 722 lower salt concentration when ω (the globule bulkiness)
 723 increases.

4. CONCLUSIONS

724 In this paper we have applied the analytical self-consistent field
 725 Poisson–Boltzmann approach to study thermodynamics of
 726 interactions between planar PE brushes and globular proteins,
 727 modeled as nanoparticles (NPs) comprising weak cationic and
 728 anionic groups on their surfaces. The position-dependent
 729 insertion free energy $\Delta F(z)$ and the net charge $Q(z)$ of the NP
 730 were calculated as a function of environmental conditions (pH
 731 and salt concentration c_s in the buffer), numbers of cationic
 732 and anionic ionizable groups on the NP surface, the NP
 733 volume V , and grafting density σ of the brush-forming
 734 polyelectrolyte chains.

735 The insertion free energy $\Delta F(z) = \Delta F_{\text{ion}}(z) + \Delta F_{\text{vol}}(z)$
 736 accounts for the position-dependent ionization contribution
 737 $\Delta F_{\text{ion}}(z)$ of NP in the electrostatic field induced by a planar PE
 738 brush, and for the work $\Delta F_{\text{vol}}(z)$ performed against excess
 739 osmotic pressure of mobile ions. As long as the electrostatic
 740 potential $\psi(z)$ induced by permanently charged (“quenched”)
 741 PE brush can be tuned by changing the ionic strength in the
 742 solution, $\Delta F_{\text{vol}}(z)$ is controlled solely by the globule volume V
 743 and the salt concentration c_s in the buffer. On the contrary,
 744 $\Delta F_{\text{ion}}(z)$ can be expressed as a function of ionization degrees of
 745 cationic, $\alpha_+(z)$ and anionic, $\alpha_-(z)$ groups that depend on both,

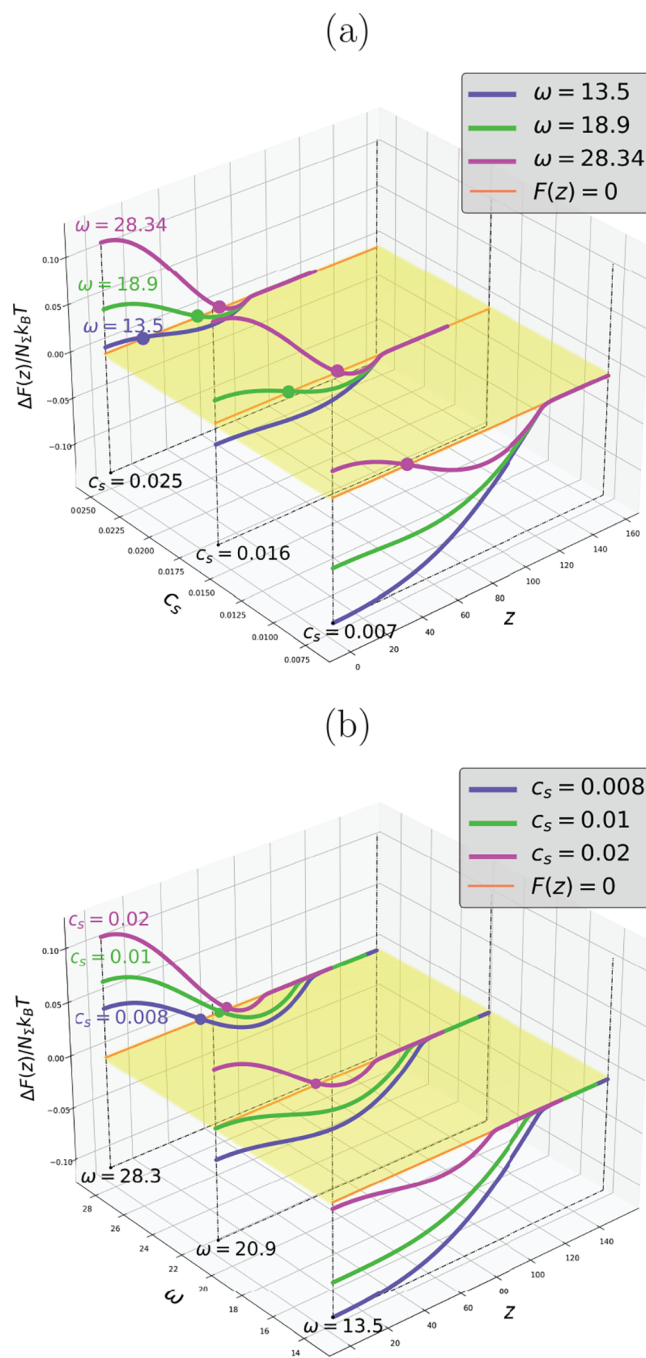


Figure 12. Cross sections of the 2D profiles of the total free energy curves $\Delta F(z, c_s) = \Delta F_{\text{ion}}(z, c_s) + \Delta F_{\text{vol}}(z, c_s)$ (a) and $\Delta F(z, \omega) = \Delta F_{\text{ion}}(z, \omega) + \Delta F_{\text{vol}}(z, \omega)$ (b), both normalized by N_s for a set values of ω corresponding to different globule volume to the number of charges ratio (a) and different salt concentrations (b), respectively (with the corresponding color code, as indicated at the curves). $s/a^2 = 100$. Colored circles in panels indicate points of vanishing free energy, $\Delta F(z, c_s) = 0$ and $\Delta F(z, \omega) = 0$.

the buffer pH_b, and the ionic strength (via $\psi(z)$). Importantly, 746
 $\alpha_-(z)$ decreases providing positive contribution to $\Delta F_{\text{ion}}(z)$, 747
 whereas $\alpha_+(z)$ increases providing negative contribution to 748
 $\Delta F_{\text{ion}}(z)$ upon insertion of NP in polyanionic brush (with the 749
 electrostatic potential $\psi(z) \leq 0$ monotonously increasing as a 750
 function of z). Generalization to the case of polycationic PE 751
 brush is straightforward by changing sign of $\psi(z)$ from negative 752
 to positive. 753

754 In calculating the insertion free energy $\Delta F(z)$ we
755 implemented a number of approximations:

- 756 (i) An uptake of NPs (protein globules) from buffer
757 solution by PE brush is presumed to occur without
758 changing the conformational state of the globule and
759 spatial distribution of electrostatic potential $\psi(z)$
760 induced by the brush. That is, NPs are considered as
761 probes. This approximation is valid at small protein
762 concentrations $c_b^{(\text{globules})}$ in buffer solution, and at no
763 strong binding of NPs to the brush-forming PE chains.
764 (ii) Small values of $c_b^{(\text{globules})} \ll 1$ allow us to specify the
765 density profiles $c_b^{(\text{globules})}(z)$ of absorbed in the brush
766 globules as

$$767 \quad c_b^{(\text{globules})}(z) = c_b^{(\text{globules})} \exp[-\Delta F(z)] \quad (32)$$

768 and the related partition coefficient,

$$769 \quad \frac{\langle c_b^{(\text{globules})} \rangle}{c_b^{(\text{globules})}} = \frac{1}{H} \int_0^H \exp[-\Delta F(z)] dz \quad (33)$$

770 The latter specifies the ratio of average concentration
771 $\langle c_b^{(\text{globules})} \rangle$ of globules inside the brush, and concentra-
772 tion $c_b^{(\text{globules})}$ in the buffer solution. The limitation
773 $c_b^{(\text{globules})} \ll 1$ is most important at $\text{pH}_b \leq \text{pH}_{\text{IEP}}$ when
774 absorption of large amounts of NPs by colloidal
775 polyelectrolyte brushes unavoidably leads to collapse of
776 the brush and loss of colloid stability. This restriction is
777 less important if PE chains are grafted to planar
778 substrates, although perturbation of the PE brush
779 structure upon absorption of large amounts of NPs
780 also brings the theory to the limit of its validity.

- 781 (iii) Reionization upon insertion is assumed to occur for all
782 N_Σ ionizable groups on NP. However, for globular
783 proteins with compact ternary structure, only amino acid
784 residues localized at the globule-water interlace are
785 involved in (re)ionization process, leading therefore to
786 concomitant renormalization of N_Σ .
787 (iv) Our approach does not account for additional attraction
788 between NP and PE brush due to charge–charge
789 correlations that provide negative contribution to the
790 insertion free energy $\Delta F(z)$. The charge–charge
791 correlations are most important for protein globules
792 with pronounced nonuniform (“patchy”) distribution of
793 cationic and anionic groups on the globule surface. In
794 the latter case, the brush-forming PE chains may adsorb
795 on the oppositely charged patches of charge, but be
796 depleted from similarly charged patches.²⁴
797 (v) Our model neglects also the short-range nonelectrostatic
798 interactions between the brush-forming PE chains and
799 the surface of NPs that could be mediated by the solvent
800 quality or temperature. In spite of the anticipated
801 dominant role of electrostatic forces, such interactions
802 should be necessarily taken into account for full
803 quantitative prediction of absorption threshold and
804 diffusion rates for specific proteins.

805 By implementing the above approximations, and using the
806 self-consistent Poisson–Boltzmann approach, we have dem-
807 onstrated that the insertion free energy profiles $\Delta F(z)$ exhibit
808 complex patterns as a function of z depending on the
809 environmental conditions (pH_b , c_s) and the globule volume
810 V normalized by the number of ionizable groups N_Σ . The
811 depth of the minima and the height of the maxima in $\Delta F(z)$

profiles are mediated by the number N_Σ of ionizable groups, 812
and the globule volume V . Notably, the implemented approach 813
allows us to specify the lower pH_b boundary for uptake of NPs 814
by PE brush. 815

The analysis of our results indicates that one can distinguish 816
three characteristic ranges of pH_b with respect to the NP 817
isoelectric point, pH_{IEP} , in the buffer: 818

$\text{pH}_b > \text{pH}_{\text{IEP}}$. The NP is strongly negatively charged in the 819
buffer, $Q_b < 0$. The NP charge Q remains negative upon 820
insertion in polyanionic brush, but decreases in magnitude 821
upon approach to the grafting surface, where the electrostatic 822
potential of PE brush is the strongest. The $\Delta F_{\text{ion}}(z)$ and $\Delta F(z)$ 823
are monotonously decreasing functions of z indicating 824
expulsion of NPs from the brush. The magnitude of the 825
repulsive free energy grows as a function of pH_b (due to the 826
increase in $|Q_b|$), but decreases upon an increase in the ionic 827
strength in the buffer solution. 828

$\text{pH}_b \geq \text{pH}_{\text{IEP}}$. The NP is charged negatively in the buffer, 829
 $Q_b \leq 0$, but acquires positive net charge upon insertion (or 830
approach to PE brush). The charge inversion, $Q(z) = 0$, occurs 831
at $z = z^*$ at which $\Delta F_{\text{ion}}(z)$ passes through a maximum. At 832
 $z \leq z^*$ the globule charge becomes positive and keeps 833
increasing whereas the ionic part of the free energy, $\Delta F_{\text{ion}}(z)$, 834
decreases reaching either positive or negative value at the 835
grafting surface, $z = 0$. For small globules, $\Delta F(0) < 0$ indicates 836
their accumulation in the brush. At $\Delta F(0) > 0$, the local 837
minimum in $\Delta F_{\text{ion}}(z)$ at the grafting surface, $z = 0$, 838
corresponds to a metastable state separated by the potential 839
barrier from the bulk of the solution. Hence, even when the 840
NP net charge changes its sign from negative to positive, 841
absorption of NPs by PE brush is not necessarily 842
thermodynamically favorable though NPs may be kinetically 843
trapped there. 844

An increase in the ionic strength of the solution weakens the 845
electrostatic potential $\psi(z)$ and hinders reionization of anionic 846
and cationic groups of the inserted in the brush NP. As a result, 847
the charge inversion point, z^* , and the corresponding 848
maximum in $F_{\text{ion}}(z)$ are displaced toward the grafting surface 849
(where the magnitude of $\psi(z)$ is larger), the free energy 850
 $\Delta F_{\text{ion}}(z = 0)$ grows and turns from negative to positive 851
indicating passing the absorption threshold. Eventually, at high 852
salt concentrations the potential $\psi(z)$ becomes too weak to 853
induce reionization of the NP inside the brush, and the NPs 854
are repelled by the brush. 855

A progressive increase in the NP volume V (an increase in 856
 ω) at constant ionic strength leads to the growth of repulsive 857
osmotic contribution $\Delta F_{\text{vol}}(z)$ at constant $\Delta F_{\text{ion}}(z)$. As a result, 858
the $\Delta F(z)$ curves are shifted upward while the position of 859
maximum, z_{max} is displaced toward the grafting surface. 860
Importantly, now the position of maximum, z_{max} does not 861
coincide with the charge inversion point, z^* , and 862
 $Q(z = z_{\text{max}}) \geq 0$. Further increase in the NP volume V leads 863
to $\Delta F(z = 0) \geq 0$ and eventual transformation of $\Delta F(z)$ into 864
monotonously decreasing curve. That is, expulsion of the bulky 865
globule from the brush in spite of the charge inversion (which 866
can be traced in the $\Delta F_{\text{ion}}(z)$ and $Q(z)$ curves). 867

$\text{pH}_b \leq \text{pH}_{\text{IEP}}$. The NP is positively charged in the buffer 868
and, therefore, attracted to the PE brush by the Coulomb 869
force. The $\Delta F_{\text{ion}}(z) \leq 0$ at all z , and the NP positive charge 870
grows upon insertion into the brush and approach to the 871
grafting surface. However, absorption of a bulky globule can be 872
hindered and even fully suppressed due to osmotic (repulsive) 873
term, $\Delta F_{\text{vol}}(z)$. An increase in the globule volume (and in 874

875 $\Delta F_{\text{vol}}(z)$) at constant salt concentration c_s leads to the increase
876 in $\Delta F(z)$ primarily in the proximal to the grafting surface
877 region, flattening of the presurface potential well, and
878 eventually leading to the appearance of the presurface
879 maximum with $\Delta F(z = 0) \geq 0$. The maximum is separated
880 from the bulk of the solution by the minimum which
881 progressively gets more shallow and narrow, and is displaced
882 to the external boundary of PE brush. A similar evolution of
883 $\Delta F(z)$ curve is observed for globules with fixed V and N_{Σ} upon
884 variations in the salt concentration. The minimum in $\Delta F(z)$ is
885 shifted toward the periphery of the brush (and progressively
886 disappears) upon an increase in c_s . The theory thereby predicts
887 that below IEP the interplay between ionic attraction and
888 osmotic repulsion may result in preferential accumulation of
889 the absorbed protein globules in the central or even peripheral
890 regions of the brush, whereas the proximal to the grafting
891 surface region is depleted from globules. This feature is most
892 attractive in design of bionanoreactors in which accumulation
893 of the proteins (enzymes) in the brush is required, but their
894 direct contacts with underlying substrate (that could lead to
895 nonspecific adsorption, denaturation, and loss of enzymatic
896 activity) should be avoided.

897 We remark that amplitudes of the minima and maxima in
898 $\Delta F(z)$ curves that determine the thermodynamic stability of
899 the protein absorbed state or the probability of overcoming the
900 potential barrier separating the absorbed state from the bulk of
901 the solution or from the grafting surface depend on the
902 number of charged groups and volume of the globule. With
903 typical values of $N_{\Sigma} \sim 10^2$, the potential well easily reaches the
904 depth of a few $k_B T$ under experimentally relevant conditions.
905 Furthermore, reionization and the NP absorption on the
906 “wrong side” of the IEP is suppressed by increasing salt
907 concentration (in full agreement with the experimental data²⁰),
908 but might be operational for sufficiently densely grafted PE
909 brushes that induce strong local electrostatic field.

910 To summarize, our theory predicts how the electrostatic and
911 osmotic parts of the insertion free energy change upon
912 insertion of ampholytic NP containing pH-sensitive acidic and
913 basic groups in a planar PE brush from the solution in a wide
914 range of the buffer pH_b . On the “wrong side” of the isoelectric
915 point, the negative balance in the free energy may be assured
916 by overcompensation of the free energy losses due to
917 suppression of ionization of similarly (with respect to the
918 brush) charged monomeric groups by gains due to enhanced
919 ionization of the oppositely charged ones, and be accompanied
920 by the change in the sign of the net charge of NP inside the
921 brush. However, the local minimum in the NP free energy
922 inside the brush may correspond to a metastable state even if it
923 is accompanied by the net charge reversal. Importantly,
924 knowledge of the insertion free energy profile $\Delta F(z)$ allows
925 also for the calculation and control of the diffusion rates of
926 NPs through the brush to be considered in our forthcoming
927 publication.

928 ■ ASSOCIATED CONTENT

929 **SI** Supporting Information

930 The Supporting Information is available free of charge at
931 <https://pubs.acs.org/doi/10.1021/acs.biomac.2c01153>.

932 Detailed derivation of the electrostatic potential
933 distribution in the planar PE brush (PDF)

934 ■ AUTHOR INFORMATION

935 Corresponding Author

Oleg V. Borisov – CNRS, Université de Pau et des Pays de
l'Adour UMR 5254, Institut des Sciences Analytiques et de
Physico-Chimie pour l'Environnement et les Matériaux,
64053 Pau, France; St. Petersburg National Research
University of Information Technologies, Mechanics and
Optics, 197101 St. Petersburg, Russia; Institute of
Macromolecular Compounds of the Russian Academy of
Sciences, 199004 St. Petersburg, Russia; orcid.org/0000-0002-9281-9093; Email: oleg.borisov@univ-pau.fr

945 Authors

Tatiana O. Salamatova – St. Petersburg National Research
University of Information Technologies, Mechanics and
Optics, 197101 St. Petersburg, Russia; orcid.org/0000-0002-7559-1824
Mikhail Y. Laktionov – St. Petersburg National Research
University of Information Technologies, Mechanics and
Optics, 197101 St. Petersburg, Russia
Ekaterina B. Zhulina – Institute of Macromolecular
Compounds of the Russian Academy of Sciences, 199004 St.
Petersburg, Russia; orcid.org/0000-0001-9139-3484

Complete contact information is available at:

<https://pubs.acs.org/10.1021/acs.biomac.2c01153>

958 Notes

The authors declare no competing financial interest.

960 ■ ACKNOWLEDGMENTS

This work was financially supported by Russian Foundation for
Basic Research, Grant 21-53-10005.

963 ■ REFERENCES

- (1) Achazi, K.; Haag, R.; Ballauff, M.; Dervedde, J.; Kizhakkedathu, J. N.; Maysinger, D.; Multhaupt, G. Understanding the Interaction of Polyelectrolyte Architectures with Proteins and Biosystems. *Angew. Chem., Int. Ed.* **2021**, *60* (8), 3882–3904.
- (2) Nie, C. A. X.; Pouyan, P.; Lauster, D.; Trimpert, J.; Kerkhoff, Y.; Szekeres, G. P.; Wallert, M.; Block, S.; Sahoo, A. K.; Dervedde, J.; Pagel, K.; Kaufner, B. B.; Netz, R. R.; Ballauff, M.; Haag, R. Polysulfates Block SARS-CoV-2 Uptake through Electrostatic Interactions. *Angew. Chem., Int. Ed.* **2021**, *60* (29), 15870–15878.
- (3) Kapelner, R. A.; Yeong, V.; Obermeyer, A. C. Molecular determinants of protein-based coacervates. *Curr. Opin. Colloid Interface Sci.* **2021**, *52*, 101407.
- (4) Yeong, V.; Werth, E. G.; Brown, L. M.; Obermeyer, A. C. Formation of biomolecular condensates in bacteria by tuning protein electrostatics. *ACS Cent. Sci.* **2020**, *6*, 2301–2310.
- (5) Kabanov, A. V.; Kabanov, V. A. Interpolyelectrolyte and block ionomer complexes for gene delivery: physico-chemical aspects. *Adv. Drug Delivery Rev.* **1998**, *30* (1–3), 49–60.
- (6) Schallon, A.; Synatschke, C. V.; Jerome, V.; Müller, A. H. E.; Freitag, R. Nanoparticulate Nonviral Agent for the Effective Delivery of pDNA and si RNA to Differentiated Cells and Primary Human T Lymphocytes. *Biomacromolecules* **2012**, *13*, 3463–3474.
- (7) Miyata, K.; Nishiyama, N.; Kataoka, K. Rational design of smart supramolecular assemblies for gene delivery: chemical challenges in the creation of artificial viruses. *Chem. Soc. Rev.* **2012**, *41*, 2562–2574.
- (8) Yu, T.; Liu, X.; Bolcato-Bellemin, A.-L.; Wang, Y.; Liu, C.; Erbacher, P.; Qu, F.; Rocchi, P.; Behr, J.-P.; Peng, L. An amphiphilic dendrimer for effective delivery of small interfering RNA and gene silencing in vitro and in vivo. *Angew. Chem., Int. Ed.* **2012**, *124*, 8606–8612.

- 994 (9) Liu, X.; Zhou, J.; Yu, T.; Chen, C.; Cheng, Q.; Sengupta, K.;
995 Huang, Y.; Li, H.; Liu, C.; Wang, Y.; Posocco, P.; Wang, M.; Cui, Q.;
996 Giorgio, S.; Fermeglia, M.; Qu, F.; Pricl, S.; Shi, Y.; Liang, Z.; Rocchi,
997 P.; Rossi, J. J.; Peng, L. Adaptive Amphiphilic Dendrimer-Based
998 Nanoassemblies as Robust and Versatile siRNA Delivery Systems.
999 *Angew. Chem., Int. Ed.* **2014**, *126*, 12016–12021.
- 1000 (10) Fan, X.; Zhao, Y.; Xu, W.; Li, L. Linear-Dendritic Block
1001 Copolymer for Drug and Gene Delivery. *Mater. Sci. Eng., C* **2016**, *62*,
1002 943–959.
- 1003 (11) Malmsten, M.; Bysell, H.; Hansson, P. Biomacromolecules in
1004 Microgels - Opportunities and Challenges for Drug Delivery. *Curr.*
1005 *Opin. Colloid Interface Sci.* **2010**, *15*, 435–444.
- 1006 (12) Bysell, H.; Mansson, R.; Hansson, P.; Malmsten, M. Microgels
1007 and Microcapsules in Peptide and Protein Drug Delivery. *Adv. Drug*
1008 *Delivery Rev.* **2011**, *63*, 1172–1185.
- 1009 (13) Hachim, D.; Whittaker, T. E.; Kim, H.; Stevens, M. M.
1010 Glycosaminoglycan-based biomaterials for growth factor and cytokine
1011 delivery: Making the right choices. *J. Controlled Release* **2019**, *313*,
1012 131–147.
- 1013 (14) Braatz, D.; Dimde, M.; Ma, G.; Zhong, Y.; Tully, M.;
1014 Grotzinger, C.; Zhang, Y.; Mavroskoufis, A.; Schirner, M.; Zhong, Z.;
1015 Ballauff, M.; Haag, R. Toolbox of Biodegradable Dendritic (Poly
1016 glycerol sulfate)-SS-poly(ester) Micelles for Cancer Treatment:
1017 Stability, Drug Release, and Tumor Targeting. *Biomacromolecules*
1018 **2021**, *22* (6), 2625–2640.
- 1019 (15) Kiani, C.; Chen, L.; Wu, Y. J.; Yee, A. J.; Yang, B. B. Structure
1020 and functions of aggrecan. *Cell Res.* **2002**, *12*, 19–32.
- 1021 (16) Cagno, V.; Tseligka, E. D.; Jones, S. T.; Tapparel, C. Heparan
1022 sulfate proteoglycans and viral attachment: True receptors or
1023 adaptation bias? *Viruses* **2019**, *11* (7), 596.
- 1024 (17) Wittemann, A.; Haupt, B.; Ballauff, M. Adsorption of proteins
1025 on spherical polyelectrolyte brushes in aqueous solution. *Phys. Chem.*
1026 *Chem. Phys.* **2003**, *5*, 1671–1677.
- 1027 (18) Wittemann, A.; Ballauff, M. Interaction of proteins with linear
1028 polyelectrolytes and spherical polyelectrolyte brushes in aqueous
1029 solution. *Phys. Chem. Chem. Phys.* **2006**, *8*, 5269–5275.
- 1030 (19) Becker, A. L.; Henzler, K.; Welsch, N.; Ballauff, M.; Borisov, O.
1031 V. Proteins and polyelectrolytes: A charge relationship. *Curr. Opin.*
1032 *Colloid Interface Sci.* **2012**, *17*, 90–96.
- 1033 (20) Walkowiak, J.; Gradzielski, M.; Zauscher, S.; Ballauff, M.
1034 Interaction of Proteins with a Planar Poly(acrylic acid) Brush:
1035 Analysis by Quartz Crystal Microbalance with Dissipation Monitoring
1036 (QCM-D). *Polymers* **2021**, *13*, 122.
- 1037 (21) Yigit, C.; Welsch, N.; Ballauff, M.; Dzubiella, J. Protein
1038 Sorption to Charged Microgels: Characterizing Binding Isotherms
1039 and Driving Forces. *Langmuir* **2012**, *28*, 14373–14385.
- 1040 (22) Biesheuvel, P. M.; Wittemann, A. A modified box model
1041 including charged polyelectrolyte brush: self-consistent field theory.
1042 *J. Phys. Chem. B* **2005**, *109*, 4209–4214.
- 1043 (23) de Vos, W. M.; Leermakers, F. A. M.; de Keizer, A.; Cohen
1044 Stuart, M. A.; Kleijn, J. M. Field theoretical analysis of driving forces
1045 for the uptake of proteins by like-charge polyelectrolyte brushes:
1046 effects of charge regulation and patchiness. *Langmuir* **2010**, *26*, 249–
1047 259.
- 1048 (24) Leermakers, F. A. M.; Ballauff, M.; Borisov, O. V. On the
1049 mechanisms of interaction of globular proteins with polyelectrolyte
1050 brushes. *Langmuir* **2007**, *23*, 237–247.
- 1051 (25) Xu, X.; Angioletti-Uberti, S.; Lu, Y.; Dzubiella, J.; Ballauff, M.
1052 Interaction of Proteins with Polyelectrolytes: Comparison of Theory
1053 to Experiment. *Langmuir* **2019**, *35*, 5373–5391.
- 1054 (26) Kim, S.; Sureka, H. V.; Kayitmazer, A. B.; Wang, G.; Swan, J.
1055 W.; Olsen, B. D. Effect of protein surface charge distribution on
1056 protein-polyelectrolyte complexation. *Biomacromolecules* **2020**, *21*,
1057 3026–3037.
- 1058 (27) Lunkad, R.; Barroso da Silva, F. L.; Kosovan, P. Both Charge-
1059 Regulation and Charge-Patch Distribution Can Adsorption on the
1060 Wrong Side of the Isoelectric Point. *J. Am. Chem. Soc.* **2022**, *144*,
1061 1813–1825.
- (28) Laktionov, M. Y.; Zhulina, E. B.; Borisov, O. V. Proteins and
1062 polyampholytes interacting with polyelectrolyte brushes and micro-
1063 gels: the charge reversal concept revised. *Langmuir* **2021**, *37*, 2865–
1064 2873.
- (29) Zhulina, E. B.; Borisov, O. V. Structure and Interactions of
1066 Weakly Charged Polyelectrolyte Brushes: Self-Consistent Field
1067 Theory. *textit J. Chem. Phys.* **1997**, *107*, 5952–5967.
- (30) Zhulina, E. B.; Klein Wolterink, J.; Borisov, O. V. Screening
1069 Effects in Polyelectrolyte Brush: Self-Consistent Field Theory.
1070 *Macromolecules* **2000**, *33*, 4945–4953.
- (31) Lebedeva, I. O.; Zhulina, E. B.; Borisov, O. V. Self-consistent
1072 Field Theory of Polyelectrolyte Brushes with Finite Chain
1073 Extensibility. *J. Chem. Phys.* **2017**, *146*, 214901–6.
- (32) Zhulina, E. B.; Borisov, O. V. Poisson-Boltzmann Theory of
1075 pH-Sensitive (Annealing) Polyelectrolyte Brush. *Langmuir* **2011**, *27*,
1076 10615–10633.
- (33) Zhulina, E. B.; Borisov, O. V. Brushes of Dendritically
1078 Branched Polyelectrolytes. *Macromolecules* **2015**, *48* (19), 1499–
1079 1508.
- (34) Zhulina, E. B.; Boulakh, A. B.; Borisov, O. V. Repulsive Forces
1081 between Spherical Polyelectrolyte Brushes in Salt-Free Solution. *Z.*
1082 *Phys. Chem. (Berlin, Ger.)* **2012**, *226*, 625–643.
- (35) Lunkad, R.; Murmiliuk, A.; Tosner, Z.; Stepanek, M.; Kosovan,
1084 P. Role of pK_a in Charge Regulation and Conformation of Various
1085 Peptide Sequences. *Polymers* **2021**, *13*, 214.
- (36) Lunkad, R.; Biehl, P.; Murmiliuk, A.; Blanco, P. M.; Mons, P.;
1087 Stepanek, M.; Schacher, F. H.; Kosovan, P. Simulations and
1088 Potentiometric Titrations Enable Reliable Determination of Effective
1089 pK_a Values of Various Polyzwitterions. *Macromolecules* **2022**, *55*,
1090 7775–7784.
- (37) Halperin, A.; Kröger, M.; Zhulina, E. B. Colloid-brush
1092 interactions: The effect of solvent quality. *Macromolecules* **2011**, *44*,
1093 3622–3638.
- (38) Merlitz, H.; Wu, C.-X.; Sommer, J.-U. Inclusion Free Energy of
1095 Nanoparticles in Polymer Brushes. *Macromolecules* **2012**, *45*, 8494–
1096 8501.
- (39) Laktionov, M. Y.; Shavykin, O. V.; Leermakers, F. A. M.;
1098 Zhulina, E. B.; Borisov, O. V. Colloidal particles interacting with a
1099 polymer brush: a self-consistent field theory. *Phys. Chem. Chem. Phys.*
1100 **2022**, *24*, 8463–8476.
- (40) Landau, L. D.; Lifshitz, E. M. *Statistical Physics*; Pergamon
1102 Press: Oxford, 1986.
- (41) RCSB PDB: Homepage. <https://www.rcsb.org> (accessed
1104 2022–08–21). 1105